Remarks:

The July 22, 2005 Official Action has been carefully considered. In view of the present amendment and these remarks, favorable reconsideration and allowance of this application are respectfully requested.

At the outset it is noted that an initial, shortened statutory response period of three (3) months was set in the July 22, 2005 Official Action. The initial due date for response, therefore, was October 22, 2005. A petition for a two (2) month extension of the initial response period is presented with this amendment and request for reconsideration, which is being filed before the expiration of the two (2) month extension period.

In the July 22, 2005 Official Action, claims 3, 4, 6, 11, 17, 19-24, 34, 35, 43, 52 and 54-56 stand rejected for allegedly failing to satisfy the enablement requirement of 35 U.S.C. §112. In support of these rejections, the examiner contends that undue experimentation would be required for one skilled in the art to implement the aspects of the invention called for in the rejected claims.

Claim 43 is rejected under 35 U.S.C. §112, second paragraph as allegedly lacking antecedent basis for certain of the subject matter recited therein.

Independent claims 1 and 36 and various claims dependent thereon have been rejected under 35 U.S.C. §102 as allegedly anticipated by:

(i) Lee et al. JACS, 124: 11850-51 (2002);

(ii) Ohba et al. Nano Letters, 1 (7): 371-73 (2001);

(iii) U.S. Patent No. 6,733,828 to Chao et al.; and

(iv) U.S. Patent Application Publication No. US2003/0148086 A1 of Pfefferle et al.

Also, claims 25-33 stand rejected under 35 U.S.C. §103 as allegedly obvious based on the combined disclosures of U.S. Patent Application Publication No. US2003/0209314 A1 of Guo et al., considered in view of the above-cited Lee et al. reference.

Claims 36-46 and 48-53 have been rejected as allegedly obvious based on the combined disclosures of U.S. Patent No. 6,746,594 to Akeson et al. and Li et al., Nature, 412: 166-69 (2001).

Claim 47 has been rejected as allegedly obvious based on the combined disclosures of the above-cited Akeson et al. and Li et al. references, considered in view of U.S. Patent No. 6,863,833 to Bloom et al.

The foregoing rejections constitute all of the grounds set forth in the July 22, 2005 Official Action for refusing the present application.

In accordance with the present amendment, claims 1 has been amended to include certain recitations set forth in original claims 2 and 3 (in part). Accordingly, claim 2 has been canceled, and consequential amendments have been made in claims 3, 4, 8-10, 13 and 15-19.

Claim 19 has been further amended to make the terminology therein cosistent with claim 1, from which claim 19 now depends.

The dependency of claim 28 has been amended so as to provide antecedent basis for certain of the recitations appearing therein.

Claim 35 has been amended so as to recite that the coated nanometer-scale conduit is approximately one nanometer in lateral dimension.

Also, the subject matter of claim 54 has been incorporated into claim 53.

Claims 5, 36-52 and 54 have been canceled in accordance with this amendment. As a result of the cancellation of claims 5, 36-52 and 54, certain of the rejections set forth in the July 22, 2005 Official Action are rendered moot. These include the 35 U.S.C. §112, first paragraph rejections of claims 43, 52 and 54, the 35 U.S.C. §112, second paragraph rejection of claim 43, all of the 35 U.S.C. §102 rejections of claims 36-39 and the 35 U.S.C. §103 rejection of claims 36-53.

The cancellation of claims 5, 36-52 and 54 should not be interpreted as indivative of applicants' concurrence or acquiescence in the various rejections of claims 5, 36-52 and 54 set forth in the July 22, 2005 Official Action, or otherwise as an abandonment of applicants' efforts to secure patent protection on the subject matter of such claims. To the contrary, applicants vigorously dispute those grounds of rejection. Such arguments as applicants have to advance in rebuttal, however, are being reserved for a continuing application, which is expected to be filed and include claims directed to some or all of the subject matter of canceled claims 5 and 36-52.

No new matter has been introduced into this application by reason of the present amendment.

For the reasons set forth below, applicants

respectfully submit that the 35 U.S.C. §112 rejections of claims 3, 4, 6, 11, 17, 19-24, 55 and 56, the 35 U.S.C. §102 rejections of claims 1, 5, 7-10, 12-16 and 18 based variously on the above-cited Lee et al., Ohba et al., Chao et al. and Pfefferle et al. references and the 35 U.S.C. §103 rejection of claims 25-33 based on the combined disclosure of the above-cited Guo et al. and Lee et al. references, as set forth in the July 22, 2005 Official Action either lack merit or cannot be maintained in view of the present amendment, or both. These grounds of rejection are, therefore, respectively traversed.

A. Claims 3, 4, 6, 11, 17, 19-24 and 54-56 Fully Satisfy The Enablement Requirement Of 35 U.S.C. §112, First Paragraph

Regarding the examiner's contention that undue experimentation would be required to practice the features of the invention claimed in claims 3, 4, 6, 11, 17, 19-24 and 54-56, it is respectfully submitted that each rejection in the July 22, 2005 Official Action based on alleged inadequate enablement must fail. The law is well-settled that whenever a rejection based on inadequacy of enablement is made, it is incumbent upon the PTO to explain why the truth or accuracy of the applicants' disclosure is doubted and to back up any such doubt with acceptable evidence or reasoning which is inconsistent with the sufficiency of the disclosure in question. In re Marzocchi, 169 U.S.P.Q. 367 (C.C.P.A. 1971). In the present case, the examiner has done no more than merely assert that undue experimentation would be required to practice the full scope of applicants' invention.

The Background of the Invention section of

applicant's specification notes certain shortcomings in existing techniques for fabrication of nano-structured devices. The examiner cites certain of these observations in support of the inadequate enablement rejections in this case. In doing so, the examiner misses the point.

Techniques for forming microchannels in a substrate, such as electron beam lithography, focused ion beam milling and nanoimprint lithography have been known for some time and are useful as far as they go. The present invention allows one to take a device having a dimension of width or depth on the order of 100 nanometers, for example, and reduce it to a smaller dimension in a controlled fashion by the application of an appropriate thickness of coating material. Several examples of ways in which coating materials may be applied or developed on nanochannel surfaces, employing different types of coating materials, are set out at pages 12-15 of the present specification.

Furthermore, the means for enclosing the nanochannel(s) with a cover member are well documented in the art. Wafer bonding is one such means, as described in Stjernstrom and Roeraade, J. Micromech. Microeng., 8: 33 (1998).

As for the examiner's query concerning how pressure or a vacuum is to be created in the uncovered nanochannel, the simple answer is that it isn't. Not all embodiments of applicants' invention, however, require the use of pressure or vacuum to impart a coating to nanochannel surfaces. See, for example, the surface modification technique described in the paragraph bridging pages 14-15 of the specification. This

technique would be applicable, for example, when implementing the method claimed in claim 3.

Concerning claims 20 and 21, the use of resist layers in the fabrication of nano-scale structures is quite common, as a Google search will readily reveal.

While the examiner correctly notes that U.S. Patents Nos. 5,858,195 and 6,001,229, which are referred to, inter alia, at page 13 of the present specification, do not disclose nanochannels, that is not the purpose for which these patents are cited. Rather, the '195 and '229 patents are cited for their disclosure of electrokinetically driving coating materials, such as the polyelectrolytes disclosed at page 13, lines 12-18, through the nanochannel(s) in order to coat the surface thereof. This coating technique would be useable, for example, when implementing the method claimed in claim 4, wherein the cover member encloses the nanochannel prior to application of the coating material. This technique would also be used in embodiments having a polyelectrolyte coating, involving alternate application of oppositely charged polyelectrolytes, as claimed in claim 17 and 34.

Regarding claim 6, the use of ion implantation to induce nano-sized particle formation on various substrates, including silicon oxide, is well known in the art, as shown, for example in U.S. Patent 6,294,223 to Hamekian et al., and references cited therein. Thus, the formation of nano-sized precipitates in the channels of the nano-structured devices claimed herein by means of non implantation cannot reasonably be regarded as involving undue experimentation.

As for claim 11, reaction schemes for covalent

immobilization of various molecules, to metal and other substrates, using diverse chemistries, have been widely reported in the literature. See, for example, the references cited by Sun and Kiang in Handbook of Nanostructured Biomaterials and Their Applications in Nanotechnology, Vols. 1-2, Chapter V, pages 1-33 (copy attached), and in particular page 4, under the heading "Attachment of DNA to surfaces". See also Lin et al, Langmuir, 18: 788-96 (2002) (copy attached). In view of such disclosures, undue experimentation would not be required of those skilled in the art in order to covalently attach DNA, for example, to a channel surface in a nanostructured device.

The points discussed above are also applicable to the practice of method claim 19, which involves the coating of a substrate having both a nanochannel and a microchannel. It is noted in this regard that the examiner concedes that techniques used in manufacturing and coating microfluidic channel were advanced and had some degree of predictability at the time of the present invention.

Turning to claim 35, as previously noted, this claim has been amended to recite that the coated nanometer-scale conduit is approximately one (1) nanometer. Applicants had no intention for claim 35 to cover a nanostructured device having a nanometer-scale conduit that starts with a lateral dimension of approximately one (1) nanometer, which is then further reduced. It is the coated (or finished) device that has a nanometer-scale conduit with a lateral dimension of approximately one (1) nanometer.

Enablement for claims 54-56, like that for claims 17

and 34 noted above, is provided by the disclosure of the above-mentioned '195 and '299 patents, which teach how to electrokinetically transport various materials through small-scale channel structures.

For the reasons given above, it is clear that the fabrication techniques, coating materials and materials of construction used to fabricate applicants' nano-structured devices are all set forth in the specification in sufficient detail to allow those skilled in the art (the level of skill in the art of nanostructured device fabrication being rather high) to successfully practice the invention as claimed. No more is required under the enablement provision of §112. Cf. In re Strahilevitz, 212 U.S.P.Q. 561 (C.C.P.A. 1982) (examples are not required to satisfy §112, first paragraph).

For all of the foregoing reasons it is respectfully submitted that the PTO clearly has failed to sustain its burden on the enablement issue. Accordingly, unless the examiner presents evidence or reasoning substantiating the doubts expressed regarding the scope of enablement provided by the present specification, the rejection of claims 3, 4, 6, 11, 17, 19-24 and 54-56 is clearly improper and should be withdrawn.

B. The Lee et al., Ohba et el., Chao et al. And Pfefferle et al. References All Fail To Anticipate The Subject Matter Of Claims 1, 5, 7-10, 12-16 And 18 As Now Amended

Rejections under 35 U.S.C. §102 are proprer only when the claimed subject matter is identically disclosed or described in the reference cited as evidence of anticipation.

In re Arkley, 172 U.S.P.Q. 524 (C.C.P.A. 1972). Applying this rule of law to the present case, the various 35 U.S.C. §102 rejections of claims 1, 5, 7-10, 12-16 and 18 based variously on the Lee et al., Ohba et al., Chao et al. and Pferrerle et al. references are improper because the subject matter of those claimed is nowhere identically disclosed or described in the cited references.

As noted above, claim 1 as now amended, calls for a three (3) step method of reducing a cross-sectional dimension of a nano-opening in a nanostructured device, including subject matter previously recited in original claims 2 and 3.

It is noted that among the references cited as evidence of anticipation in the July 22, 2005 Official Action, only the Pfefferle et al. reference was applied in rejecting claim 2; and none was applied in rejecting claim 3.

Inasmuch as neither Lee et al. or Ohba et al. or Chao et al. or Pfefferle et al. identically discloses or describes all of the claim recitations of applicants' claims 1, 5, 7-10, 12-16 and 18, the §102 rejection of such claims based on those four (4) reference is untenable and should be withdrawn.

C. The Combined Disclosures Of The Guo et al. And Lee et al. References Fail To Render Obvious The Subject Matter Of Claims 25-33

As noted by the PTO Board of Appeal in Ex parte Wolters, 214 U.S.P.Q. 735 (Bd. Apps. 1979), the burden of establishing a *prima facie* case of obviousness falls upon the examiner. In determing whethere a case of prima facie obviousness exists, it is necessary to ascertain whether or not the disclosures of the cited prior art reference would

appear to be sufficient to motivate one or ordinary skill in the art to make the claimed substitution, combination or other modification. In re Litner, 173 U.S.P.Q. 560 (C.C.P.A. 1972). Merely because it is possible to find two (2) prior art disclosures which might be combined in such a way as to arrive at the claimed subject matter does not make the combination of disclosures obvious, unless the art also contains something to suggest the desirability of the proposed combination. In re Imperato, 179 U.S.P.Q. 730 (C.C.P.A. 1973).

In the present case, there is nothing to suggest the desirability of combining the disclosures of the Guo et al. and the Lee et al. references in the manner proposed by the examiner.

Guo et al. describes a method of forming nanofluidic channels, which involves providing a first substrate having a layer of a first material disposed thereon. According to the detailed description of Guo et al., the first material is a polymer. A plurality of nanoscale slots is formed along a second substrate by means of nanolithography, etching or other disclosed techniques. Among the specific channel-forming techniques disclosed in Guo et al., are electron beam lithography, deep UV lithography, nanoprinting technique and reactive ion etching. The first substrate is then bonded to the second substrate, such that the layer of the first material on the first substrate is adjacent to the plurality of slots on the second substrate to define a plurality of enclosed nanofluidic channels therethrough.

The stated object of the invention of Guo et al. is to provide "a simple method of fabricating nanofluidic

channels with dimensions down to tens of nanometers, which facilitates low-cost and high-volume manufacturing of nanofluidic channels for a wide range of applications".

Lee et al., on the other hand, relates to Au nanotube membranes (Au-NTMs) and their use in electromodulated molecular transport. It is evident that the phenomenon of electromodulated neutral molecule transport described in Lee et al. relies on the electrically conductive nature of the Au-NTMs. Indeed, an electrical potential of appropriate charge is applied to the Au-NTMs in order to cause partitioning of the anionic surfactant into the nanotube, which is a necessary step in effecting the desired molecular transport. The nanofluidic channels of Guo et al., by contrast, are not disclosed as being electrically conductive, nor is there any apparent reason why one of ordinary skill in the art would want to make them so. Such additional processing would certainly be contrary to the stated objective of Guo et al., namely, facilitating low-cost and high-volume manufacturing of nanofluidic channels.

Moreover, the electro-osmotic flow applications apparently contemplated by Guo et al. (which are referred to by the examiner at page 54 of the July 22, 2005 Official Action) do not require an electrically conductive conduit, which is essential for the application described by Lee et al. Electro-osmosis, as is well known, results from the surface charge of materials, such as silicon oxide from which the nanostructured devices of the present invention may be fabricated. When a voltage is applied across a nanometer-scale conduit made of silicon oxide, the cation species

present on the conduit surface are attracted to the cathode. Because they are solvated, they drag the bulk solution behind them as they move through the conduit. Thus, the devices of Guo et al. have no need of a coating of the type used in Lee et al. in order to effect electro-osmotic flow through their naonfluidic channels.

It is also noteworthy that although Guo et al. is concerned with control of dimensions in nanofluidic channels, the approach provided by Guo et al. for achieving such control is very specific. It is done by controlling the initial thickness of the layer of polymer material and/or the initial width or depth dimension of slots fabricated in the second substrate. See paragraph 0020 of Guo et al.

Lee et al., by contrast, is not at all concerned with modifying the dimensions of the Au-NTMs described therein. Thus, it is not at all evident why one of ordinary skill in the art would be motivated by the disclosure of Lee et al. to coat the nanofluidic channels of Guo et al. in the manner proposed by the examiner. Such a modification would certainly be contrary to the fabrication scheme devised by Guo et al. for low-cost and high-volume manufacturing of nanofluidic channels. Given that the proposed modification essentially undermines the purpose of the primary reference, this proposed combination of prior art references would not have been obvious to one of ordinary skill in the art. See, Ex parte Hartmann, 186 U.S.P.Q. 366 (Bd. Apps. 1974).

The obviousness rejection of claims 25-33 based on the combined disclosures of Guo et al. and Lee et al. is clearly premised on a hindsight reconstruction of the claimed

invention. It is quite apparent that the Examiner has used applicants' disclosure as a guide for combining unrelated prior art teachings in an effort to make out a case of *prima facie* obviousness. Such hindsight reconstruction has long been held impermissible, however, since it is contrary to the standard of obviousness set forth in the 35 U.S.C. §103, which requires a determination of whether the claimed subject matter as a whole would have been obvious at the time the invention was made, based on the state of the art as reflected in the cited references, and without benefit of applicants' disclosure. Ex parte Stauber, 208 U.S.P.Q. 945 (Bd. Apps. 1980). Neither of the references relied on by the Examiner in support of the §103 rejection of claims 25-33 contains the slightest suggestion to use what is disclosed in one reference in combination with what is disclosed in the other references. Cf. In re Avery, 186 U.S.P.Q. 161 (C.C.P.A. 1975). That being the case, it cannot reasonably be maintained that the combined disclosures of Guo et al. and Lee et al. fairly suggest doing what the applicants herein have done.

Inasmuch as the references cited in support of the §103 rejection of claims 25-33 fail to teach or suggest the claimed subject matter as a whole, it necessarily follows that the prior art fails to render the subject matter of claims 25-33 *prima facie* obvious. Accordingly, the rejection of claims 25-33 under 35 U.S.C. §103 based on the combined disclosures of Guo et al. and Lee et al. is improper and should be withdrawn.

In view of the amendment presented herewith and the foregoing remarks, it is respectfully urged that the

rejections set forth in the July 22, 2005 Official Action be withdrawn and that this application be passed to issue, and such action is earnestly solicited.

Respectfully submitted,

DANN, DORFMAN, HERRELL & SKILLMAN
A Professional Corporation
Attorneys for Applicant(s)

By Patrick J. Hagan

Patrick J. Hagan
PTO Registration No. 27,643

Telephone: (215) 563-4100
Facsimile: (215) 563-4044

Attachments:

- Sun and Kiang in Handbook of Nanostructured Biomaterials and Their Applications in Nanotechnology, Vols. 1-2, Chapter V, pages 1-33 "Attachment of DNA to surfaces"

- Lin et al, Langmuir, 18: 788-96 (2002)

DNA Attachment and Hybridization at the Silicon (100) Surface

Zhang Lin, Todd Strother, Wei Cai, Xiaoping Cao, Lloyd M. Smith, and Robert J. Hamers*

Department of Chemistry, University of Wisconsin, 1101 University Avenue, Madison, Wisconsin 53706

Received June 12, 2001. In Final Form: October 9, 2001

The chemical modification of silicon surfaces for DNA attachment and subsequent hybridization has been investigated using X-ray photoelectron spectroscopy and contact angle measurements, in conjunction with fluorescence-based measurements of DNA hybridization. The feasibility of using small molecules to functionalize Si surfaces with primary amine groups for DNA attachment has been explored using the free amine 1-amino-3-cyclopentene (ACP) and a modified molecule with a protecting group on the amine, *N*-1-BOC-amino-3-cyclopentene (BACP). Direct attachment of amines leads to chemically heterogeneous surfaces, while the use of suitable protection and deprotection chemistry can produce a homogeneous surface with a high density of primary amine groups. The resulting amine-terminated surfaces were covalently coupled to thio-oligonucleotides using a heterobifunctional cross-linker. Hybridization experiments revealed that these DNA exhibit excellent stability to hybridization conditions, high specificity for recognition, and high density for hybridization. The ability to detect single-base mismatches is demonstrated. Factors controlling the stability, selectivity, and density of surface-bound DNA molecules are discussed.

(1) Introduction

Research on DNA-modified surfaces has become increasingly active in recent years and is anticipated to have a broad-based impact on a number of emerging biotechnology areas, such as DNA chip technologies and DNA computing.[1−3] Although many different types of surfaces have been used as substrates for DNA attachment, the need for reproducible, stable surfaces has placed increased emphasis on the preparation of DNA-modified surfaces that are extremely homogeneous.

Recent studies have shown that crystalline silicon can be used as a starting point for preparing DNA layers exhibiting a high specificity and a high density of binding sites.[4−6] Crystalline silicon has a number of potential advantages as a substrate for DNA immobilization. Starting with hydrogen-terminated silicon surfaces,[7,8] it is possible to form well-defined organic films through direct Si−C covalent bond formation.[9−12] Perhaps more importantly, the use of crystalline silicon substrates provides the potential for taking full advantage of existing microelectronic technologies associated with the silicon semiconductor industry, which can be used for highly parallel microfabrication and, in principle, direct electronic detection of biomolecular binding processes.[3,13]

Recent experiments have shown that well-defined DNA layers can be prepared on the common (100) and (111) surfaces of silicon.[4,5] In both cases, attachment was achieved by first using a long-chain alkene terminated with a reactive functional group. In one case, attachment began by attaching a long-chain ester to the surface which was then hydrolyzed to a carboxylic acid group, converted to an amine via electrostatic bonding with polylysine, and finally linked to DNA using the hetero-bifunctional cross-linker sulfo-succinimidyl 4-(*N*-maleimidomethyl) cyclohexane-1-carboxylate (SSMCC).[4] A simpler scheme[5] used direct attachment of a long-chain molecule terminated with a protected amine, which was then converted to a free amine and linked to DNA with SSMCC. In these and most other studies of DNA-functionalized surfaces, the first step has been attachment of a long-chain organic molecule to the surface. While such long-chain molecules might provide improved stability against oxidation or other undesired reactions at the interface, it is also possible that such long-chain molecules might decrease the quality of the interface through entanglement. In emerging applications involving direct electronic detection of DNA hybridization processes, however, the use of a shorter linking layer may be beneficial.[13,14]

Ideally, one would like to identify the simplest chemical scheme for linking DNA to silicon substrates in a way that achieves the highest selectivity, sensitivity, and stability in subsequent hybridization steps. We report here an integrated study in which core-level photoelectron

* Corresponding author. Phone: 608-262-6371. Fax: 608-262-0453. E-mail: rjhamers@facstaff.wisc.edu.

(1) Wang, L. M.; Liu, Q. H.; Corn, R. M.; Condon, A. E.; Smith, L. M. *J. Am. Chem. Soc.* **2000**, *122*, 7435−7440.
(2) Liu, Q.; Wang, L.; Frutos, A. G.; Condon, A. E.; Corn, R. M.; Smith, L. M. *Nature* **2000**, *403*, 175−179.
(3) Vo-Dinh, T.; Cullum, B. *Fresenius J. Anal. Chem.* **2000**, *366*, 540−551.
(4) Strother, T.; Cai, W.; Zhao, X.; Hamers, R. J.; Smith, L. M. *J. Am. Chem. Soc.* **2000**, *122*, 1205−1209.
(5) Strother, T.; Hamers, R. J.; Smith, L. M. *Nucleic Acids Res.* **2000**, *28*, 3535−3541.
(6) Lenigk, R.; Carles, M.; Ip, N.; Sucher, J. *Langmuir* **2001**, *17*, 2497−2501.
(7) Kinoshita, S.; Ohta, T.; Kuroda, H. *Bull. Chem. Soc. Jpn.* **1976**, *49*, 1149.
(8) Higashi, G. S.; Chabal, Y. J.; Trucks, G. W.; Raghavachari, K. *Appl. Phys. Lett.* **1990**, *56*, 656−658.
(9) Wagner, P.; Nock, S.; Spudich, J. A.; Volkmuth, W. D.; Chu, S.; Cicero, R. C.; Wade, C. P.; Linford, M. R.; Chidsey, C. E. D. *J. Struct. Biol.* **1997**, *119*, 189−201.
(10) Sieval, A. B.; Demirel, A. L.; Nissink, J. W. M.; Linford, M. R.; Maas, J. H. v. d.; Jeu, W. H. d.; Zuilhof, H.; Sudhölter, E. R. J. *Langmuir* **1998**, *14*, 1759−1768.
(11) Linford, M. R.; Fenter, P.; Eisenberger, P. M.; Chidsey, C. E. D. *J. Am. Chem. Soc.* **1995**, *117*, 3145−3155.
(12) Terry, J.; Linford, M. R.; Wigren, C.; Cao, R.; Pianetta, P.; Chidsey, C. E. D. *J. Appl. Phys.* **1999**, *85*, 213−221.
(13) Vo-Dinh, T.; Alarie, J. P.; Isola, N.; Landis, D.; Wintenberg, A. L.; Ericson, M. N. *Anal. Chem.* **1999**, *71*, 358−363.
(14) Janata, J. *Analyst* **1994**, *119*, 2275.

10.1021/la010892w CCC: $22.00
Published on Web 01/10/2002

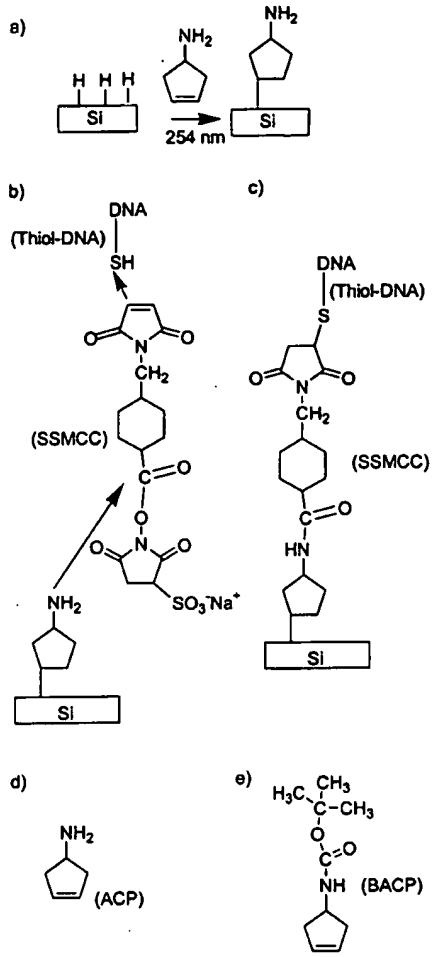

Figure 1. Overview illustrating the entire attachment process on Si(100) surfaces.

spectroscopy is used to optimize the formation of chemically modified Si(100) surfaces, and fluorescence measurements are used to assess the selectivity, stability, and sensitivity in subsequent hybridization studies. Our results show that, provided the surface chemistry is well-controlled, short, rigid linkers can also be used for DNA immobilization with good sensitivity, selectivity, and reversibility in subsequent hybridization processes. However, protection and deprotection of the amine group is critical to form chemically homogeneous layers. With optimized chemistry, we demonstrate the ability to detect even single-base mismatches. Our results also provide insight into the factors controlling these important variables.

(2) Experimental Section

(A) Overview. Figure 1 provides an overview of the overall scheme for attachment of DNA to the crystalline silicon surface. The procedure is based upon the fact that bare silicon surfaces will react readily with C=C double bonds,[15] while silicon surfaces that have their exposed Si atoms bonded to hydrogen atoms (hydrogen-terminated Si surfaces) are unreactive. Hydrogen termination was accomplished by dipping the silicon wafers in a solution of 1% hydrofluoric acid, which removes any oxidized silicon from the surface and bonds H atoms to the exposed unsaturated Si "dangling bonds". Starting with a (unreactive) hydrogen-terminated surface, local sites of reaction are defined by locally removing the H-passivation using ultraviolet light (here, at 254 nm), which then links the functionalized molecule of interest at the illuminated site. Because the bare silicon surface can also potentially react with other parts of the molecule (such as the unprotected amine group), we investigated attachment of "protected" and "unprotected" amines. Covalent linking with thiol-terminated DNA is then achieved using a hetero-bifunctional cross-linker such as SSMCC.

All reagents were purchased from commercial sources at the highest grade available. 1-Amino-3-cyclopentene (ACP), which has both an alkene group and a primary amine functionality, was purchased from Asta Tech. A protected version, in which one of the H atoms attached to the NH_2 group is replaced with a *tert*-butyl oxycarbonyl protecting group to yield the protected amine *N*-1-BOC-amino-3-cyclopentene (BACP), was also purchased from Asta Tech. Sulfo-succinimidyl 4-(*N*-maleimidomethyl) cyclohexane-1-carboxylate (SSMCC), used to link the amine-terminated surface to thiol-terminated DNA, was also purchased from Pierce Chemical. Silicon samples oriented to expose the (100) crystal face were purchased from Virginia Semiconductor; n-type (arsenic-doped) samples were used for the studies reported here. 18 MΩ-cm water from a Millipore system was used for rinsing the samples.

Oligonucleotides were synthesized by the University of Wisconsin Biotechnology Center and purified by high-pressure liquid chromatography immediately before use. Oligonucleotides to be covalently attached to the surfaces were thiol-modified at the 5′-end using the reagent 5′-thiol-modifier C6 (HSC6, Glen Research). The four sequences employed were 5′-HSC6-T_{15}AA CGA TCG AGC TGC AA-3′ (S1), 5′-HSC6-T_{15}AA CGA TGC AGG AGC AA-3′ (S2), 5′- HSC6-T_{15}AG GAA TGC CGG TTA T-3′ (S3), and 5′-HSC6-T_{15}AG GAT TGC CGG TTA T-3′ (S4). Complementary oligonucleotides used for hybridization were modified with fluorescein on the 5′-end using 6-FAM phosphoramidite (Applied Biosystems, Inc.). The three sequences employed were 5′-FAM-TT GCA GCT CGA TCG TT-3′ (F1, complementary to S1), 5′-FAM-TT GCT CCT GCA TCG TT-3′ (F2, complementary to S2), and 5′-FAM-AT AAC CGG CAT TCC T −3′ (F3, complementary to S3 and with a single-based mismatch to S4). Immediately before use, the thiol-oligonucleotides were deprotected according to guidelines from Glen Research[16] and then purified by reverse-phase HPLC. The thiol-oligonucleotides (for surface functionalization) were used at a concentration of approximately 1 mM while their fluorescent complements (for hybridization) were used at a concentration of 2 μM. Hybridization and rinsing buffer used during the studies was referred to as 2×SSPE/0.2% SDS, which consists of 2 mM EDTA, 7 mM sodium dodecyl sulfate, 300 mM NaCl, and 20 mM NaH_2PO_4 with pH = 7.4.

(B) Optimized Preparation of DNA-Modified Silicon Surfaces. Si wafers were ultrasonically cleaned in acetone and methanol for 5 min each, followed by oxidation in a solution prepared by mixing 30% hydrogen peroxide, 28−30% ammonium hydroxide, and water in a 1:1:4 volumetric ratio. After soaking for 5 min at 75 °C, the Si samples were dipped briefly in a 1% HF solution to remove the oxidized layer and were rinsed in water to remove any residual fluorine, producing hydrogen-terminated Si surfaces.[4,9] Because H-terminated Si surfaces will oxidize slowly at atmospheric pressure, they were used as soon as possible after preparation and kept under a nitrogen atmosphere whenever possible.

The BACP molecule is a solid at room temperature. To prepare a uniform solid layer on the Si−H surface, 50 μL of BACP in methanol (50 mg/mL) was spread on a surface area of approximately 1 cm^2, and a thin film formed by evaporation of the solvent. The sample was then irradiated with 254-nm ultraviolet light to induce the desired alkene attachment reaction; a period of 1.5−2 h was the optimal reaction time. Physically absorbed BACP molecules were removed by sonicating the samples twice in CH_3Cl and once in methanol, for 5 min each.

The optimal reaction conditions for deprotection of the amine group were established using contact angle measurements to

(15) Hamers, R. J.; Coulter, S. K.; Ellison, M. D.; Hovis, J. S.; Padowitz, D. F.; Schwartz, M. P.; Greenlief, C. M.; Russell, J. N., Jr. *Acc. Chem. Res.* **2000**, *33*, 617−624.

(16) *User Guide to DNA Modification*; Glen Research Corporation: 1996.

rapidly assess the chemical changes, in conjunction with more detailed XPS measurements. The optimized procedure for deprotection was determined to be immersion into 25% trifluoroacetic acid in CH_2Cl_2 for 2 h, followed by 10% NH_4OH for 5–7 min.[5] This procedure is similar to that previously optimized for deprotection of a t-BOC-protected alkeneamine.[5] The resulting amine-terminated surfaces were then allowed to react with a hetero-bifunctional cross-linker.

Although we compared several linkers, SSMCC was used most extensively. SSMCC was linked to the amine-modified Si(100) surface by covering the surface with 50 μL of a solution of SSMCC (1.5 mM in 150 mM triethanolamine buffer, pH 7) for 20 min. The DNA was then linked to the SSMCC-terminated surface by applying 0.4–0.8 μL droplets of ~1 mM thiol-oligonucleotides to the surface and allowing the reaction to continue overnight. Two other linkers, *N*-succinimidyl iodoacetate (SIA) and sulfosuccinimidyl(4-iodoacetyl) aminobenzoate (SSIAB) were also evaluated.

To use these linkers, 1.4 mg of SIA or 1.7 mg of sulfo-SIAB was dissolved into 1 mL of PBS buffer solution (0.1 M sodium phosphate, 0.15 M NaCl, pH 7.2).[17] The resulting SIA or SIAB solution was dripped onto the amine-terminated surface and kept in the dark, producing surfaces terminated with the thiol-reactive iodoacetyl group. Thiol-modified oligonucleotides were then deposited onto the surface and allowed to couple with the iodoacetyl group in the dark for at least 20 h.

Chemical characterization of the surface modification chemistry was performed using X-ray photoelectron spectroscopy (XPS) measurements and water contact angle measurements. XPS spectra were obtained using an Al Kα source (1486.9 eV photon energy) and a 16-channel detector. XPS spectra were analyzed using standard curve-fitting procedures in which the quality of fit was evaluated through a "quality-of-fit" parameter, based on a reduced χ^2. A smaller value for the reduced χ^2 represents a better fit, with values of less than 1 indicating that the fit and the data are indistinguishable within the experimental noise. The static water contact angle measurements were carried out on an NRL goniometer (Ramé-hart 100) with an error of ±2°.

The detailed procedures for hybridizing the fluorescent complements to the surface-immobilized thiol-oligonucleotides have been described previously.[4,18] Briefly, the thiol-oligonucleotide modified surfaces were placed in 5–10 μL of 2 μM 5′-fluorescein-labeled complement and allowed to hybridize for 20 min in a humid chamber at room temperature. These hybridized surfaces were soaked twice in 2×SSPE/0.2% SDS buffer for a total of 10 min to rinse off any physically adsorbed oligonucleotides. A Molecular Dynamics FluorImager 575 was then used to visualize and quantify the fluorescence intensity from the modified silicon surfaces. These images were scanned after putting the silicon wafers face down in a droplet of 2×SSPE/0.2% SDS buffer on the FluorImager tray. Subsequent denaturation was performed by placing the surfaces in a 8.3 M urea solution at 37 °C for 5–10 min. The surfaces were then rinsed with water and rescanned with the FluorImager. After ensuring a complete denaturation, subsequent hybridizations could be redone using the same procedure.

(3) Results

(A) Chemical Attachment of Protected and Non-protected Amines to the Si(100) Surface. The studies presented here focus primarily on two methods of attaching amine groups to silicon surfaces. Figure 1d depicts the molecule 1-amino-3-cyclopentene (ACP). This molecule contains a reactive alkene group and an unprotected, primary amine group. Because of the possibility that a primary amine group might react directly with the Si surface, we also investigated protecting the amine with the *tert*-butyloxycarbonyl (*t*-BOC) group. For simplicity, we refer to the resulting protected molecule *N*-1-BOC-amino-3-cyclopentene as BACP; the structure of the BACP

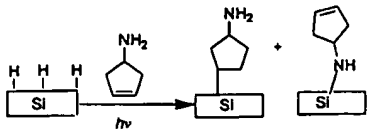

Figure 2. Reaction pathways for ACP interacting with the silicon substrate.

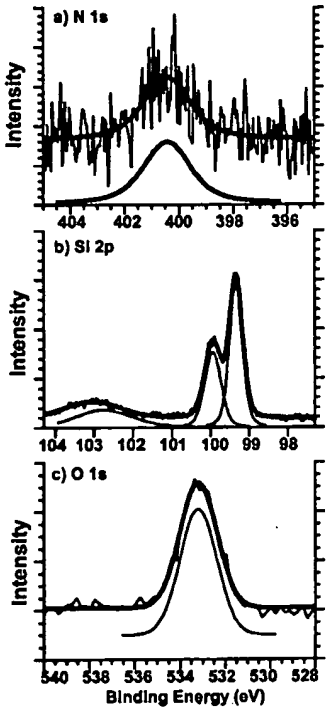

Figure 3. X-ray photoelectron spectra of the nitrogen (1s), silicon (2p), and oxygen (1s) core levels from the Si(100) surface modified by ACP.

molecule is shown in Figure 1e. Both the ACP and BACP molecules contain a reactive alkene (C=C group). Since alkene groups are known to react with the Si(100) surface via the photochemical process used here,[5] we anticipate that both molecules can, in principle, bind to the surface via the alkene group. However, as shown in Figure 2, since amines might also react with the surface, a comparison of the protected and unprotected amines was carried out to help identify how to best protect against such undesired side reactions.

To attach the ACP molecule to the surface, 250 μL of ACP was deposited onto a 1 cm^2 region of a hydrogen-terminated Si(100) surface. The surface and the thin liquid film were then illuminated with UV light (254 nm) for 1.5 h under a dry nitrogen atmosphere. Figure 3 shows the resulting X-ray photoelectron spectra in the regions corresponding to the nitrogen (1s), silicon (2p), and oxygen (1s) core levels. The N(1s) spectrum in Figure 3a shows a weak peak with a binding energy of 400.4 eV and a breadth of 2.2 eV, measured as the full-width at half-maximum (fwhm). The Si(2p) spectrum in Figure 3b shows two sharp peaks at 99.4 and 100.0 eV and a much broader peak at higher binding energy, extending from 102 to 104 eV. Finally, Figure 3c shows the oxygen 1s spectrum of this surface, revealing a peak at a binding energy of 533.2 eV. More quantitative information can be obtained from analysis of the peak areas, using the Si(2p) bulk as an internal standard. In Figure 3, the area of the N(1s) peak is 0.85 times the total area of the Si(2p) spectrum, while the area of the O(1s) peak is 3.9 times the total area of

(17) Hermanson, G. T. *Bioconjugate Techniques*; Academic Press: San Diego, 1996.

(18) Frutos, A. G.; Smith, L. M.; Corn, R. M. *J. Am. Chem. Soc.* **1998**, *120*, 10277–10282.

the Si(2p) region. The broad 102−104 eV Si peak constitutes 25% of the total area of the Si(2p) spectrum.

We consider first the Si spectrum. In XPS measurements, spin−orbit splitting causes the 2p levels from each Si atom to split into $2p_{1/2}$ and $2p_{3/2}$ components, in a 1:2 intensity ratio. The two peaks at 99.4 and 100.0 eV arise from a single chemical form of silicon and correspond to the well-known binding energy of unreacted, bulk silicon. The broader peak at 102−104 eV, however, can be attributed to silicon atoms in more positive oxidation states than those in the bulk. Silicon oxidized by O_2 and/or H_2O gives rise to peaks at 102−104 eV due to SiO_2, SiO, and SiOH groups.[19-23] Likewise, we attribute the broad features in this region to oxidized Si atoms. Since the total area in the 102−104 eV range is approximately 0.25 times the total Si(2p) area, this suggests that ~25% of the silicon atoms within the sampling volume are oxidized.

The 400.4 eV N(1s) peak is higher in energy and also broader than those observed for other amines. For example, in studies of primary and secondary amines, we have found N(1s) binding energies near 398.8 eV for C−NH−Si moieties and 399.4 eV for C−NH−C moieties, with a fwhm near 1.0 eV.[24] Similarly, ammonia (NH_3) produces a N(1s) peak at 399.1 eV from Si−NH_2 species. The comparatively high energy and broad width of the N(1s) peak from ACP suggest an inhomogeneous distribution of binding sites, with the N atoms in comparatively electron-deficient environments. More importantly, analysis of the peak intensities shows that the N groups are present in low concentration. The absolute N coverage can be determined quantitatively by comparison with XPS measurements performed on this same instrument under conditions identical to those for the NH_3 molecule, which is known to dissociate into a single NH_2 fragment and an adsorbed H atom on each dimer of the Si(100) surface.[25] In most experiments reported here the N and Si signals are recorded using slightly different conditions (specifically, different pass energies) to provide the best balance between sensitivity and resolution. By performing similar measurements (not shown) on NH_3 and ACP under identical instrumental conditions, we find that the N/Si ratio of ACP is approximately 0.4 times the N/Si ratio produced by NH_3 adsorption. This then corresponds to an N coverage of approximately 0.2 nitrogen atom per surface Si atom. A similar value can be crudely determined from the known atomic sensitivity factors for N and Si and correcting for the finite escape depth of the photoemitted electrons. Finally, the amount of oxidation can be approximately determined. On the basis of the 1486 eV excitation, the relative sensitivities in the XPS measurements for Si, N, and O are 0.27, 0.42, and 0.66, respectively. The O(1s) spectrum shows a single, fairly strong peak at 533.1 eV. This binding energy is intermediate between the value ~533.7 eV usually associated with Si−O linkages and the value ~532.3−532.6 eV associated with Si−O−Si linkages.[20,23] While physisorbed water can also give rise to a peak at this energy, the existence of the 102−104 eV peaks in the silicon XPS spectrum indicates that silicon oxidation is substantial. Integrating the area under the peak yields an O/Si area ratio of 3.9; this corresponds to approximately 4.5 O atom per N atom, or approximately one oxygen atom per surface Si atom.

The XPS data presented in Figure 3 show that direct attachment of ACP via the photochemical scheme results in extensive surface oxidation, with relatively poor attachment of ACP. Similar results (not shown) have also been obtained for attachment of 10-aminodec-1-ene, a long-chain alkeneamine. Thus, we conclude that molecules containing unprotected amine groups cause extensive oxidation and poor attachment. The use of protecting groups is limited by the fact that many protecting groups can only be deprotected under harsh conditions that can also significantly alter the silicon substrate. Since silicon surfaces can be etched under both acidic and basic aqueous solutions,[26] neither acid-labile nor base-labile protecting groups are clearly preferable. In a previous study we found that protecting groups that require strongly basic conditions tend to cause surface oxidation unless a physically large base, such as potassium *tert*-butoxide, is used, and we obtained the best results using the acid-labile, t-BOC protecting group.[4] Consequently, we investigated the attachment and subsequent modification of the Si(100) surface with BACP.

Following the experimental procedures outlined above, Figure 4 shows XPS data for the nitrogen (1s), silicon (2p), and carbon (1s) core levels of the Si (100) surface at various stages of chemical modification. We first present two control experiments. The first panel (Figure 4a) shows the spectra of a control sample that was H-terminated. The H-terminated surface shows no N contamination, and only a small C signal that is presumably due to physically adsorbed hydrocarbons, as this peak decreases in intensity upon mild heating. Panel 4b shows data from a sample that was H-terminated and then covered with BACP as described above, but *not* subjected to UV illumination. In this case, the N(1s) spectrum shows a weak peak with a binding energy of 400.5 eV and a fwhm of 1.50 eV. The carbon (1s) spectrum shows two weak peaks with binding energies of 284.9 and 286.6 eV. The Si(2p) spectrum in Figure 4b shows two sharp peaks at 99.4 and 100.0 eV but shows no significant intensity at the higher binding energies of 102−104 eV that are characteristic of oxidized silicon. Measurement of the N and Si peak areas yields a N/Si peak area ratio of 0.24.

Finally, Figure 4c shows a sample that was H-terminated, covered with BACP, and then exposed to UV for 2 h. The N(1s) spectrum has a single peak with a binding energy of 400.5 eV and a width of 1.6 eV fwhm. This peak is much narrower than the 2.2 eV width observed from attachment of the unprotected ACP molecule to the Si(100) surface. This narrower width indicates that the chemical homogeneity of the amine groups is significantly improved. In fact, the 1.6 eV width is identical to that observed from NH_3 and other amines when prepared under pristine ultrahigh vacuum conditions on silicon surfaces.[24] Quantitative analysis of the peak areas yields a ratio of N to Si peak areas of 3.0. This can be compared with the value of 0.85 observed for the unprotected ACP molecule under identical instrumental operating conditions. Again, on the basis of comparison of the N/Si ratio for BACP layers with similar measurements for NH_3 adsorption,[25] the surface N density of the BACP-modified surface is approximately 1 N atom per surface Si atom, or approximately 6×10^{14}

(19) Himpsel, F. J.; McFeely, F. R.; Taleb-Ibrahimi, A.; Yarmoff, J. A.; Hollinger, G. *Phys. Rev. B* **1988**, *38*, 6084−6096.
(20) Prabhakaran, K.; Kobayshi, Y.; Ogino, T. *Surf. Sci.* **1993**, *290*, 239−244.
(21) Hollinger, G.; Himpsel, F. J.; Hughes, G.; Jordan, J. L. *Surf. Sci.* **1986**, *168*, 609−616.
(22) Chambers, J. J.; Parsons, G. N. *Appl. Phys. Lett.* **2000**, *77*, 2385−2387.
(23) Namiki, A.; Tanimoto, K.; Nakamura, T.; Ohtake, N.; Suzaki, T. *Surf. Sci.* **1989**, *222*, 530−534.
(24) Cao, X.; Coulter, S. K.; Ellison, M. D.; Liu, H.; Liu, J.; Hamers, R. J. *J. Phys. Chem. B* **2001**, *105*, 3759−3768.
(25) Dresser, M. J.; Taylor, P. A.; Wallace, R. M.; Choyke, W. J.; Yates, J. T. J. *Surf. Sci.* **1989**, *218*, 75−107.
(26) Yang, S. K.; Peters, S.; Takoudis, C. G. *J. Appl. Phys.* **1994**, *76*, 4107−4112.

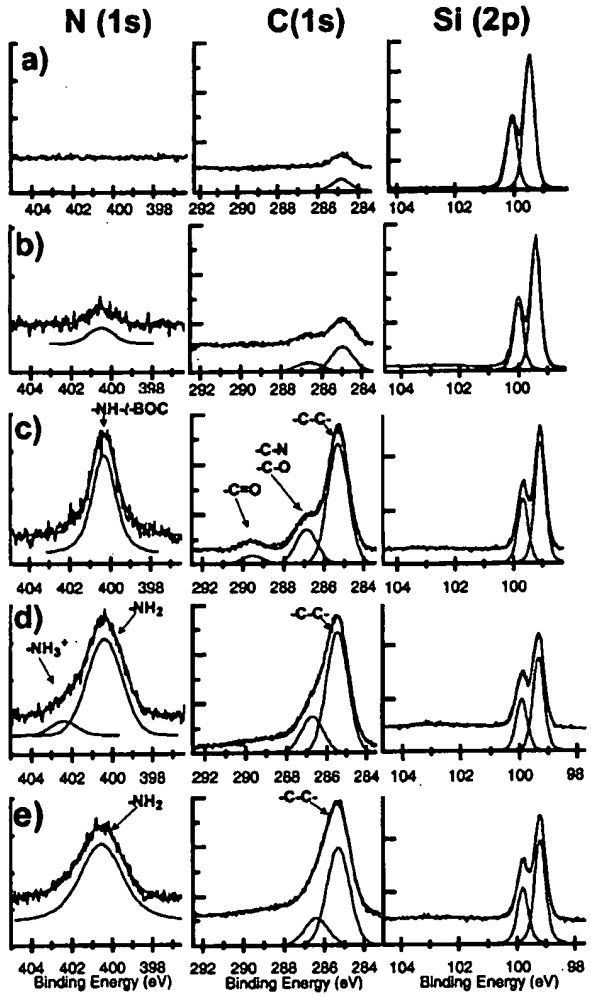

Figure 4. XPS spectra at various stages of chemical modification: (a) H-terminated Si(100) sample; (b) H-terminated Si(100) sample that was covered with BACP but not exposed to UV light; (c) H-terminated Si(100) sample that was covered with BACP and illuminated for 2 h with UV light; (d) Si(100) surface modified by BACP and then exposed to 25% trifluoroacetic acid (TFA) in CH_2Cl_2 for 2 h; (e) identical sample to that for part d, after subsequent treatment with 10% NH_4OH for 7 min.

N atoms/cm^2. We also note that the N/Si peak area ratio obtained on the sample that was covered with BACP and illuminated with UV is more than 12 times larger than that from the sample that was not illuminated with UV. This demonstrates that UV illumination greatly facilitates the attachment process.

Since later stages in the attachment process require chemically accessible amine groups, understanding the chemical nature of these N atoms is also important. Previous studies have shown that bonding of saturated primary amines such as 1-hexylamine leads to direct Si–N bond formation, with N(1s) binding energies of 398.8–399.0 eV.[24,27] In contrast, previous experiments of free NH_2 groups have reported N(1s) binding energies of 399.5–400.5 eV.[28] The value of 400.5 eV we observe for BACP therefore suggests that the amine group is not bonded directly to the Si surface, suggesting that the protected amine group is unaffected by the surface attachment. Analysis of the other core level leads to similar conclusions. The C(1s) spectrum in Figure 4b shows a large peak at 285.3 eV and two smaller peaks at 287.0 and 289.7 eV. In a previous study of a surface-bonded trifluoroethyl ester,[4] we found that the carbon in the C=O group gave rise to a peak at 289.3 eV, while the ether-like carbon (C–O) had a binding energy of 287.5 eV. Similarly, for BACP we attribute the peak at 289.7 eV to the carbon atom in the carbonyl group, the peak at 287.0 eV to the carbon atom in the ether linkage (C–O) and possibly the C atoms bonded to N, and the large peak at 285.3 eV to the alkane-like carbon atoms. Thus, the C(1s) spectrum strongly suggests that the attachment of BACP to the Si surface leaves the *t*-BOC protecting group intact.

Finally, we note that the Si(2p) spectrum in Figure 4b shows only two peaks, with little or no intensity in the 102–104 eV region. The absence of peaks in the 102–104 eV region (cf. Figure 3b) also indicates that there is no significant oxidation of the underlying Si surface. Although interpretation of the O(1s) spectrum is often complicated by adsorption of trace amounts of water, the O(1s) spectrum (not shown) exhibits two O(1s) peaks, at 533.9 and 532.5 eV, with nearly identical integrated areas. The peak at lower binding energy is similar to that observed for carbonyl groups and is therefore attributed to the C=O of the t-BOC group; the peak at higher binding energy (533.9 eV) is attributed to the ether-like C–O group. These binding energies are similar to those in previous studies, which reported 531.5–532.2 eV for C=O groups and 533.2–534.0 eV for oxygen atoms in ether-like (C–O–C) linkages.[29–31]

(B) Deprotection of BACP. The above experiments show that the protected amine BACP attaches to the Si surface with a much higher density and in a more homogeneous manner than the unprotected amine (ACP). While unprotected silicon surfaces oxidize rapidly in the presence of base,[32] the monolayer film of attached BACP molecules acts as a protecting layer. Figure 4 shows the XPS spectra of the BACP-modified Si surface (Figure 4c), the same sample after exposure to 25% trifluoroacetic acid (TFA) in CH_2Cl_2 for 2 h (Figure 4d), and then the same sample after a subsequent exposure to10% NH_4OH for 7 min (Figure 4e). Comparing the spectra in Figure 4c with those in Figure 4d shows that exposure to TFA reduces the N(1s) peak at 400.6 eV and introduces a peak at 402.4 eV, close to the binding energy of 403.2 eV associated with ammonium-like N atoms in compounds such as NH_4Cl.[24] Figure 4e shows that subsequent exposure to 10% NH_4OH leaves most of the peaks unchanged, except that the N(1s) peak at 402.4 eV is eliminated and replaced by a new peak at 400.6 eV, close to the binding energy observed for the molecule before deprotection. These trends in binding energy, including the 1.7 eV shift associated with the protonated amine, are nearly identical to those reported in a recent study with a t-BOC protected 10-aminodec-1-ene, a similar long-chain linear molecule.[5] The chemical changes inferred from the N(1s) spectra during the deprotection steps are also reflected in the C(1s) spectra. In particular, we note that the C(1s) peak in Figure 4c at 289.7 eV, which we attributed above to the carbonyl carbon, disappears after exposure to TFA (Figure 4d). This disappearance is consistent with the loss of the *t*-BOC protecting group via acid hydrolysis in TFA. The

(27) Hovis, J. S.; Lee, S.; Liu, H.; Hamers, R. J. *J. Vac. Sci. Technol. B* **1997**, *15*, 1153–1158.
(28) Moulder, J. F. S. W. F.; Sobol, P. E.; Bomben, K. D. In *Handbook of X-day Photoelectron Spectroscopy*; Chastain, J., King, R. C., Jr., Eds.; Physical Electronics, Inc.: Eden Prairie, 1995.
(29) Bubert, H.; Lambert, J.; Burba, P. *Fresenius J. Anal. Chem.* **2000**, *368*, 274–280.
(30) Patnaik, A.; Li, C. O. *J Appl. Phys.* **1998**, *83*, 3049–3056.
(31) Hutt, D. A.; Leggett, G. J. *Langmuir* **1997**, *13*, 2740–2748.
(32) Wind, R. A.; Hines, M. A. *Surf. Sci.* **2000**, *460*, 21–38.

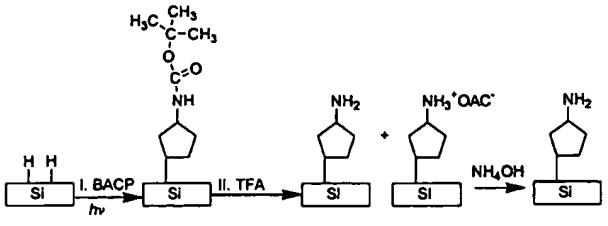

Figure 5. Reaction scheme for BACP deprotection.

Table 1. Measured Contact Angles for Si(100) Surfaces at Various Stages of the Surface Bonding Reaction of *N*-1-BOC-amino-3-cyclopentene (BACP) and the Deprotection Reactions (T = 298 K; relative humidity 25%)

surface	contact angle, θ (deg)
Si–H surface	76.0
t-BOC-protected amine	80.9
TFA treated	62.4
TFA and NH_4OH treated	70.0

nitrogen atom remains intact, and the high binding energy of 402.4 eV indicates that it is in an ammonium-like chemical form; subsequent exposure to NH_4OH restores the free primary amine (NH_2). Thus, the XPS measurements indicate that TFA can effectively deprotect the amine group, while the subsequent treatment with NH_4OH produces the free amines (NH_2).

Equally significant is the fact that the absence of any significant XPS intensity in the Si(2p) region at 102–104 eV shows that this route to amine-functionalized silicon takes place with little or no oxidation of the Si surface. From the XPS data, we conclude that while the direct attachment of the primary amine via the ACP molecule leads to poorly defined surfaces, the attachment of the protected amine BACP followed by deprotection leads to a homogeneous, amine-functionalized silicon surface, as illustrated in Figure 5.

As a further confirmation of the chemical changes observed in XPS, we also performed water contact angle measurements at each step. These data are shown in Table 1. The hydrogen-terminated surface is quite hydrophobic, with a water contact angle of 76.0°. After attachment of the *t*-BOC-protected amine, the contact angle increases to 80.9°, indicating an even more hydrophobic surface. After subsequent acid hydrolysis via exposure to 25% TFA for 2 h, the contact angle of the surface dropped to 62.4°, which can be attributed to the fact that the surfaces were now terminated with the mixture of more hydrophilic free amine and amine salt. Treatment with NH_4OH increases the contact angle to 70.0°, indicating that NH_4OH treatment converts the (hydrophilic) protonated amine (NH_3^+) into the primary amine (NH_2).

(C) Attachment of DNA to Amine-Modified Si(100) Surfaces. The above experimental results demonstrate that BACP can be attached to the Si substrate and then deprotected to form the desired primary amine-terminated surfaces. Attachment of single-stranded DNA is achieved using a hetero-bifunctional cross-linker. In this study, we evaluated three different bifunctional cross-linkers. All three link to the amine-terminated surface by forming an amide bond, but they differ in how they link to the thiol-terminated DNA. Figure 6 summarizes the linker chemistry. As depicted in Figure 6a, SSMCC reacts with amine groups through its *N*-hydroxysuccinimide ester and results in a maleimide-activated surface, which can further react with the thiol group of thiol-oligonucleotides. SIA and SIAB have C–I bonds that react readily with thiol-terminated DNA, as depicted in Figure 6b and c.

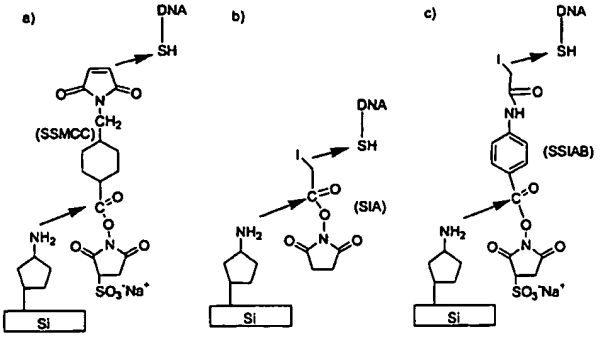

Figure 6. Summary of the use of SSMCC, SIA, and SSIAB to link thiol-terminated DNA with the amine-terminated silicon surface.

After these linkers were attached to the amine-modified surfaces, single-stranded DNA oligonucleotides (sequences S1 and S2) were bonded to the linkers, and the resulting DNA-modified surfaces were hybridized with the fluorescently tagged sequences F1 and F2. When the DNA-modified surfaces were hybridized with their complements, the resulting fluorescence intensities were nearly identical for all three linkers. The variation in fluorescence intensity was less than 30% in replicate experiments with all three linkers. No significant intensity was observed from the mismatched sequences. These results suggest that all three linkers are essentially equivalent in performance. However, in preliminary studies in which surfaces are exposed to repeated hybridization and denaturation sequences, SSMCC appears to be more stable. Consequently, subsequent experiments on the stability and selectivity toward DNA hybridization were performed using only this cross-linker.

To understand the factors limiting the density of attached DNA molecules, we also performed quantitative measurements of the density of SSMCC molecules by comparing the N(1s) intensity before and after reaction of SSMCC with the amine-terminated surface. These measurements showed that the N(1s) intensity nearly doubled after reaction with SSMCC. Since each SSMCC molecule has two nitrogen atoms, this implies that the density of surface-bound SSMCC molecules is approximately half the density of amine sites. Because the XPS intensities may be affected by the finite escape depth of the electrons through the SSMCC layer, this value should be considered only as an approximation. However, it is clear that the number density of SSMCC molecules is comparable to the density of free amines.

(D) Surface Properties in DNA Immobilization. *(i) Surface Stability to Multiple Hybridizations.* To test the stability and accessibility of the surface, we performed experiments in which the fluorescent complements and the surface-immobilized oligonucleotides were successively hybridized and denatured 13 times. In each cycle, the sample was hybridized with its complement, and the fluorescence intensity was measured using the Fluorimager; the DNA was then denatured in 8.3 M urea solution at 37 °C for 5–10 min, followed by a water rinse. The fluorescence intensity of the denatured surface (which ideally should be zero) was then measured again with the Fluorimager. Figure 7a shows the fluorescence intensities measured during each hybridization cycle. The fluorescence intensity obtained after hybridization is quite high, and in each cycle it drops to nearly zero after exposure to urea; this indicates that the urea does effectively denature the surface and that the fluorescent complements that leave the surface do not contribute to the fluorescence

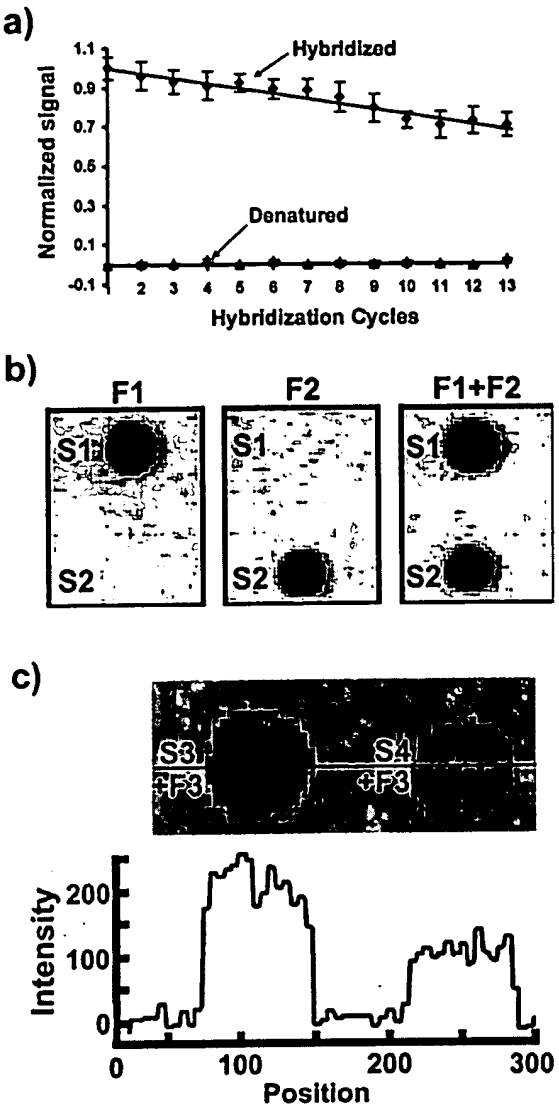

Figure 7. (a) Surface stability toward multiple hybridization and denaturation cycles. Error bars reflect error estimates from measurements on three replicate samples. (b) Fluorescence measurements (black = high intensity) of hybridization of surface-bound DNA with fluorescently labeled oligonucleotides. Two different oligonucleotides with a four-base difference (out of 16) were first attached to the surface at the spots indicated. (left) Fluorescence image of surface after hybridization with fluorescent oligonucleotides F1, complementary to sequence S1. (center) Same surface, after denaturing and hybridizing the surface with fluorescent oligonucleotides F2, complementary to sequence S2. (right) Same surface, after denaturing and hybridizing the surface with both fluorescent oligonucleotides simultaneously. (c) Fluorescence measurements of single-base mismatches in DNA hybridization. Two different 16-base oligonucleotides (S3 and S4) with a single-base difference were first attached to the surface. The image shows the intensity of fluorescence after oligonucleotide F3, complementary to S3, was hybridized on the surface.

signal. There is a small decrease in the intensity of the fluorescence in successive cycles. After 13 cycles the maximum fluorescence signal is approximately 75% of that obtained on the first cycle, corresponding to a decrease of approximately 2% per cycle.

The 2% per cycle decrease we observed is comparable to that obtained in recent studies in which DNA was attached to the Si(100) surface by first preparing an ester-terminated surface, hydrolyzing to the acid form, depositing polylysine to produce an amine-terminated surface, and then using SSMCC to link DNA to the surface.[4] Thus, we can conclude that using BACP to form the amine-terminated surface leads to surfaces that are equally robust, while the BACP procedure involves fewer steps than the previous method. Since the presence of multiple charged groups in polylysine may increase its propensity for nonspecific adsorption, we believe that the BACP molecule may provide better specificity. However, we also note that the 2% decrease in fluorescence intensity using BACP chemistry is larger than that observed in another recent study in which the long-chain alkeneamine (*t*-BOC-10-aminodec-1-ene) was used, on the (111) surface of silicon.[5] In that case the fluorescence intensity decreased by only 1% per cycle.

(ii) Density of Active Sites Accessible to DNA Hybridization. A useful surface requires bound oligonucleotides arranged on the surface with enough interstitial space to allow high hybridization efficiency. To quantitatively determine the number of surface-bound DNA molecules, we performed a calibration using gel electrophoresis and comparing the fluorescence intensities with known standards.[4,18] In this calibration procedure, single-stranded DNA was attached to the Si(100) surface as described above; the fluorescently tagged complement was then hybridized with the surface-bound DNA, and the fluorescence was measured as described above. The hybridized surfaces were then placed into 1 mL of water at 90 °C for 15 min to denature the duplex, and the fluorescent complements were collected. The denatured solution containing the complements was then reduced to a 10 μL volume using a vacuum spin-drier and loaded on one lane of a polyacrylamide gel. Fluorescent DNA standards were loaded into the other lanes. After electrophoresis, the gel was scanned and the total fluorescent signals were measured. Using this method, we determined that the density of hybridized molecules was approximately 6.0×10^{12} per cm^2, close to the value reported previously on other substrates including silicon,[4] self-assembled monolayer silane films on fused silica,[33] SiO_2,[34] and gold.[35]

(iii) Binding Specificity in DNA Hybridization. To evaluate the binding specificity, we performed experiments comparing the binding of surface-bound DNA with perfect complements as well as controlled mismatches. To illustrate general hybridization specificity, two spots of 31-mer thiol-oligonucleotides (sequences S1 and S2) with a four-base difference were applied to the SSMCC modified surface to form two circular areas approximately 2 mm in diameter. The surface was then exposed to a solution containing the fluorescently tagged sequence F1, which is complementary to S1. After 20 min of hybridization, the surface was washed and the fluorescence signal from the surface was measured. The left panel of Figure 7b shows the fluorescence images (black = high fluorescence intensity), indicating binding of F1 to the region functionalized with the S1 sequence and not to the S2 sequence. After the surface was denatured with urea and then exposed to sequence F2, fluorescence was observed only on the spot where DNA with the S2 sequence was bonded (middle panel, Figure 7b). Finally, after the surface was denatured and then exposed to an equimolar mixture of

(33) Chrisey, L. A.; Lee, G. U.; O'Ferrall, E. C. *Nucleic Acids Res.* **1996**, *24*, 3031–3039.
(34) Lamture, J. B.; Beattie, K. L. B.; Eggers, M. D.; Ehrlich, D. J.; Fowler, R.; Hollis, M. A.; Kosicki, B. B.; Reich, R. K.; Smith, S. R.; Varma, R. S.; Hogan, M. E. *Nucleic Acids Res.* **1994**, *22*, 22121–2125.
(35) Jordan, C. E.; Frutos, A. G.; Thiel, A. J.; Corn, R. M. *Anal. Chem.* **1997**, 4939–4947.

F1 and F2, fluorescence was observed from both spots with equal intensity.

To test whether the chemistry is sufficiently selective to distinguish a mismatch of only a single base pair, experiments were conducted using the sequences S3 and S4 (which differ by only a single base) and their 15-mer complements, sequences F3 and F4. As above, sequences S3 and S4 were attached to the surface in two areas, and the DNA-modified surface was then exposed to a solution containing F3. After 20 min of hybridization, the surface was washed and the fluorescence was measured. Figure 7c shows the resulting fluorescence image and the intensity profile along the indicated line. Although some binding is observed on both spots, the fluorescence signal was much stronger on its complement (S3) than on the single base pair mismatch (S4). Quantitative analysis of the fluorescence intensities shows that the average intensity (in arbitrary units) in the mismatched spot S4 + F3 was 119 (standard deviation 19), the intensity in the perfect match S3 + F3 was 239 (standard deviation 19), and the background level of the surrounding region was 5.4 (standard deviation 6). The difference in intensity between the perfect match and the single-base mismatch is 120, more than 4 times the combined standard deviation of 27. Thus, we conclude that the chemistry described here is sufficient to be able to identify a single-base mismatch with excellent discrimination.

Our experiments are largely based upon the precept that improved surface chemistry can lead to improved sensitivity and selectivity in DNA hybridization. To illustrate this, we note that the XPS data indicate that use of the unprotected amine ACP leads to extensive surface oxidation, with relatively little attachment of ACP. To identify how this affects the subsequent hybridization chemistry, we also did a control experiment in which we attempted to link thiol-terminated DNA to the ACP-modified surface using the SSMCC linker using the same procedure described above. When the fluorescently labeled complementary sequence was applied, the resulting fluorescence intensity was 107 with a standard deviation of 66, while the background regions yielded an average intensity of 112 with a standard deviation of 83. Thus, we conclude that no detectable amount of DNA hybridizes to the surfaces prepared using the unprotected amine ACP.

(4) Discussion

Optimization of surface chemistry for surface-based analysis of biomolecules such as DNA requires careful attention to the chemistry of DNA attachment in order to maximize the density of DNA binding sites, while retaining high selectivity against sequences with small numbers of mismatches. Degradation of the interface may occur during the initial attachment chemistry or during the subsequent hybridization and denaturation processes. Our research is focused on identifying the specific chemical and structural factors that lead to robust DNA-functionalized surfaces, to develop attachment chemistries that are simple and reproducible.

One general scheme for attachment of DNA to surfaces has focused on the direct bonding of alkenes containing functional groups, such as esters, acids,[4,10] and chlorides,[11] to hydrogen-terminated silicon surfaces. Previously, we have found that molecules with carboxylic acid groups will react directly with the surface but that carboxylic acid-terminated Si surfaces can be readily prepared by linking alkenes bearing an ester functionality first and then hybridizing this to the carboxylic acid after surface attachment. Similarly, the results presented here show that the direct attachment of alkenes that also bear a primary amine group leads to poorly defined attachment. Indeed, amines are widely used in the microelectronics industry for etching of silicon, and primary amines are widely known to promote the reaction of silicon with water.[36] Although our amines do not have water present intentionally, most amines are hygroscopic and readily acquire more than sufficient water to permit formation of several monolayers of oxidation products. Thus, we believe that the extensive oxidation we observe using the unprotected amine likely arises from a similar amine-enhanced reaction with trace amounts of water. However, protecting the amine with the t-BOC group reduces the basicity of the amine and apparently also reduces or eliminates its oxidizing effect on the Si surface. By utilizing the protected amine, it is possible to prepare a surface with a high density of reactive amine groups.

Our results show that the number density of amine groups is much higher than the density of DNA molecules that can ultimately be hybridized to the surface. The density of amine groups formed using BACP is approximately 6×10^{14} molecules/cm^2. In comparison, recent studies of aminosilanes have shown densities of approximately 4×10^{14} amines/cm^2.[37] Studies of the attachment of functionalized alkenes to silicon via a thermal process have also yielded attachment densities of $\sim 4 \times 10^{14}$ amines/cm^2.[10] Although these estimates indicate a slightly higher amine density using BACP than with alternative methods, this difference is not likely to be significant. Quantiative XPS analysis of the N(1s) levels shows that the SSMCC linkers are also present at comparable number densities, while hybridization and fluorescence measurements show no appreciable difference between the three different linkers employed. The number density of hybridized DNA molecules ($\sim 6 \times 10^{12}$ cm^{-2}) is typically much smaller than the number of amine sites ($\sim 6 \times 10^{14}$ cm^{-2}). This suggests that either (1) only a small number of DNA molecules are actually linked to the SSMCC molecule or (2) only a small fraction of the surface-bound DNA molecules hybridize with their complement. Our experimental data do not allow us to distinguish between these possibilities. However, it is clear that the density of DNA molecules that can ultimately hybridize with the surface is not limited by any of the initial stages of the surface modification chemistry.

The above studies show that the level of nonspecific adsorption on these silicon surfaces is sufficiently low that one can clearly distinguish mismatches of only a single base pair out of 16. Nonspecific adsorption arises from a number of possible factors, including van der Waals' forces, polarization forces created by charged groups or dipoles on the surface, and physical entanglement. Most previous studies have prepared amine-terminated surfaces via a polylysine layer that is electrostatically bonded to an acid-terminated surface, and have typically used long-chain molecules containing 12–18 carbon atoms as a "spacer" layer between the surface and the molecules of interest. Our results show that it is possible to prepare equally good layers using shorter molecules. The thickness of these functionalization layers and any subsequent linkers may help to minimize nonspecific adsorption by reducing the possibility of entanglement of DNA molecules. Additionally, it could be quite important for true integration of biomolecules with silicon to achieve (for example) direct electronic detection of hybridization processes. The po-

(36) Finne, R. M.; Klein, D. L. *J. Electrochem. Soc.* **1967**, *114*, 965–970.

(37) Moon, J. H.; Shin, J. W.; Kim, S. Y.; Park, J. W. *Langmuir* **1996**, *12*, 4621–4624.

tential drawback of the thin BACP layers is that the BACP layer is sufficiently thin that chemical degradation of the interface may be more facile. In the experiments reported here, we observed about 2% degradation in fluorescence intensity per cycle during multiple-hybridization experiments. This is slightly larger than the loss of only ~1% observed using the long-chain alkene amines such as *t*-BOC-10-aminodec-1-ene.[5] Since the (111) surface of silicon is known to be microscopically flatter and more uniform than the (100) surface used in the study presented here, this difference may simply reflect the intrinsic differences in the microscopic structure and chemistry of these different crystal faces.[38] Further careful comparisons will be required to determine whether these differences in stability arise from intrinsic differences in the chemistry or in the different atomic structures of the (111) and (100) surfaces of silicon. Additionally, the N(1s) peak from BACP is somewhat broader than the similar peak using t-BOC-10-aminodec-1-ene, suggesting a possibly greater degree of chemical degradation for BACP. Further work still needs to be done to explore and develop optimized chemical pathways for surface attachment of short organic linkers and, particularly, to identify the chemical pathways involved in the interfacial degradation.

(5) Conclusions

Covalent bonding of DNA to crystalline silicon substrates yields interfacial layers showing high selectivity in subsequent hybridization processes. Analysis of the chemical structure of the films via core-level photoelectron spectroscopy permits optimization of the chemical processing steps, yielding DNA-functionalized Si surfaces that are selective and stable toward multiple hybridization cycles. Our results show that initial attachment of protected amines, followed by subsequent deprotection of the surface-bound molecules, produces amine-terminated surfaces that are more homogeneous and have a higher density of free amine sites than surfaces produced by alternative methods involving direct attachment of unprotected amines. This improvement in homogeneity, combined with the use of a hetero-bifunctional cross-linker such as SSMCC, leads to formation of DNA-functionalized silicon surfaces exhibiting good selectivity and stability. Even short-chain amines can form DNA-functionalized surface layers exhibiting good selectivity, capable of identifying a single-base mismatch out of 16 bases, but the stability of the interface with repeated hybridizations is slightly less than that obtained using longer chain, protected alkeneamines. The residual degradation of the interface during repeated hybridization steps requires further investigation.

Acknowledgment. This work was supported in part by the National Institutes of Health, Human Genome Program Grant 1R21-HG02101-01.

LA010892W

(38) Dumas, P.; Chabal, Y. J.; Jakob, P. *Surf. Sci.* **1992**, *269/270*, 867–878.

(Invited) **Chapter V** *in "Handbook of Nanostructured Biomaterials and Their Applications in Nanobiotechnology,"* **Vols. 1-2** (ISBN: 1-58883-033-0), *edited by Nalwa, American Scientific Publishers (2005).*

DNA-based Artificial Nanostructures: Fabrication, Properties, and Applications

Young Sun and Ching-Hwa Kiang*

Department of Physics & Astronomy, Rice University

6100 Main Street - MS61, Houston, TX 77005, USA

Phone: (713) 348-4130, Fax: (713) 348-4150, E-mail: chkiang@rice.edu

Keywords: DNA; nanostructure; self-assembly; nanoparticle; carbon nanotube; biosensor.

*To whom correspondence should be addressed: chkiang@rice.edu.

Table of Content

1. Introduction

The integration of nanotechnology with biology and bioengineering is producing many advances. The essence of nanotechnology is to produce and manipulate well-defined structures on the nanometer scale with high accuracy. Conventional technologies based on the "top-down" approaches, such as the photolithographyic method, are difficult to continue to scale down due to real physical limitations including size of atoms, wavelengths of radiation used for lithography, and interconnect schemes. While engineers and scientists have long aspired to controllably manipulate structures at the micrometer and nanometer scale, nature elegantly performs these tasks and assembles structures with great accuracy and high efficiency using specific biological molecules.

Biological molecules, such as DNA, have shown great potential in fabrication and construction of nanostructures and devices. DNA molecules can be used for the assembly of devices and computational elements, for the assembly of interconnects, or as the device element itself. There are several advantages to use DNA for these constructions. First, DNA is the molecule whose intermolecular interactions are the most readily programmed and reliably predicted: Docking experiments reduce to the simple rules that A pairs with T, and G pairs with C. Thus, the very properties that make DNA so effective as genetic material also make it an excellent molecule for programmed self-assembly. Second, DNA of arbitrary sequences is available by convenient solid support synthesis. The needs of the biotechnology industry have also led to reliable chemistries to produce modifications, such as biotin groups, fluorescent labels, and linking functions. Third, DNA can be manipulated and modified by a large battery of enzymes that include DNA ligases, restriction endonucleases, kinases, and exonucleases.

On the other hand, nanotechnology has helped the development of novel biosensors for biological and medical applications. Nanobioconjugates that consists of various functional nanoparticles linked to biological molecules have been used in many areas such as diagnostics, therapeutics, sensors, and bioengineering. Detection methods based on these nanobioconjugates show increased selectivity and sensitivity as compared with many conventional assays that rely on molecular probes.

This paper reviews recent progress in the area of DNA-based artificial nanostructures. The fabrication, properties, and applications of various DNA-based nanostructures are described. New ideas and directions on DNA nanotechnology are presented. In addition, we discuss the optical and melting properties of the DNA-linked gold nanoparticles.

2. DNA fundamentals

DNA is the basic building block of life. Hereditary information is encoded in the chemical language of DNA and reproduced in all cells of living organisms. The double-stranded helical structure of DNA is key to its use in self-assembly applications. Each strand of the DNA is about 2 nm wide and composed of a linear chain of four possible bases (adenine, cytosine, guanine, and thymine) on a backbone of alternating sugar molecules and phosphate ions. Each unit of a phosphate, a sugar molecule, and base is called a nucleotide and is about 0.34 nm long. The specific binding through hydrogen bonds between adenine (A) and thymine (T), and cytosine (C) and guanine (G) can result in the joining of two complementary single-stranded DNA to form a double-stranded DNA. There are two hydrogen bonds between A-T pairs and three hydrogen bonds

between G-C pairs. The phosphate ion carries a negative charge in the DNA molecule, which results in electrostatic repulsion of the two strands. In order to keep the two strands together, positive ions must be present in the solution to keep the negative charges neutralized. The joining of two complementary single strands of DNA through hydrogen bonding to form a double-stranded DNA is called hybridization. If a double-stranded DNA is heated above a certain temperature, the two strands will start to dehybridize and eventually separate into single strands. The center temperature of this transition is called the melting temperature, T_m, which is a sensitive function of environmental conditions such as ionic strength, pH, and solvent conditions. As the temperature is reduced, the two strands will eventually come together by diffusion and rehybridize to form the double-stranded structure. These properties of the DNA can be utilized in the ordering and assembly of artificial structures if these structures can be attached to DNA.

3. Attachment of DNA to surfaces

The first step toward DNA-based nanotechnology is to attach DNA molecules to surfaces. So far, the most widely used attachment scheme utilizes the covalent bond between sulfur and gold [1-7]. Nuzzo and Allara first reported the formation of long chain ω-substituted dialkyldisulfide molecules on a gold substrate [1]. Bain et al. [5] demonstrated a model system consisting of long-chain thiols that adsorb from solution onto gold to form densely packed, oriented monolayers. The bonding of the sulfur head group to the gold substrate is in the form of a metal thiolate, which is a very strong bond (~ 44 kcal/mol), and hence the resulting films are quite stable and very suitable for surface attachment of functional groups. For example, the DNA molecule can be functionalized with a thiol (S-H) or a disulfide (S-S) group at the 3' or 5' end. Hickman et al. also demonstrated the selective and orthogonal self-assembly of disulfide with gold and isocyanide with platinum [6]. It should be noted that there are also other strategies to attach DNA to surfaces, for example, the covalent binding of DNA oligonucleotides to a preactivated particle surface [8] and adsorption of biotinylated oligonucleotides on a particle surface coated with avidin [9, 10]. These attachment schemes have served as the fundamental base for DNA-related self-assembly of artificial nanostructures.

4. Self-assembly and construction of nanostructures using DNA

There has been a tremendous interest in recent years to develop concepts and approaches for self-assembled systems. While significant work continues along this direction, it has also been recognized that the exquisite molecular recognition of various natural biological materials can be used to form a complex network of potentially useful particles for a variety of optical, electronic, and sensing applications. This approach can be considered a bottom-up approach rather than the top-down approach of conventional scaling. DNA is a particularly promising candidate to serve as a construction material in nanotechnology. Despite its simplicity, the highly specific Watson-Crick hydrogen bonding allows convenient programming of artificial DNA receptor moieties. The power of DNA as a molecular tool is enhanced by automated methods and by the PCR technique to amplify any DNA sequence from microscopic to macroscopic quantities. Another attractive feature of DNA is the great mechanical rigidity of short double helices,

so that they behave effectively like a rigid rod spacer between two tethered functional molecular components on both ends. Moreover, DNA displays a relatively high physicochemical stability. Finally, nature provides a complete toolbox of highly specific enzymes that enable the processing of the DNA material with atomic precision and accuracy.

4.1 Nanostructures of pure DNA

Seeman and co-workers [11] were the first to exploit DNA's molecular recognition properties to design complex mesoscopic structures based solely on DNA. In their work, branched DNA was used to form stick figures by properly choosing the sequence of the complementary strands. Macrocycles, DNA quadrilateral, DNA knots, Holliday junctions, and other structures were designed. Fig. 1 shows a four-armed stable branched DNA junction made by DNA molecules and the use of the branched junctions to form periodic crystals [12]. The same group also reported the design of two-dimensional crystalline forms of DNA double crossover molecules that are programmed to self-assemble by the complementary binding of the sticky ends of the DNA molecules [13]. These lattices can also serve as scaffolding material for other biological materials. A detailed review on this topic can be found in Ref. [14].

Other researchers also have put effort on using DNA to design complex architectures. Bergstrom and co-workers have designed rigid tetrahedral linkers with arylethynylaryl spacers to direct the assembly of attached oligonucleotide linker arms into novel DNA macrocycles [15]. Unlike Seeman's approach where the DNA serves as both the vertices and the edges of the assembled architectures, Bergstrom's approach utilizes rigid tetrahedral organic vertices, where the attached oligonucleotides serve as the connectors for the design of more complex architectures. In principle, a variable number of oligonucleotide arms could be attached to the core tetrahedral organic linkers, thereby allowing for the construction of different types of DNA structures.

4.2 DNA-based assembly of metal nanoparticles

In 1996, Mirkin and co-workers [16] first described a method of assembling colloidal gold nanoparticles into macroscopic aggregates using DNA as linking elements. As illustrated in Fig. 2, this method involved attaching noncomplementary DNA oligonucleotides to the surfaces of two batches of gold particles capped with thiol groups, which bind to gold. When another oligonucleotide which is complementary to the two grafted sequences is introduced, the nanoparticles self-assemble into aggregates. This process could also be reversed when the temperature was increased due to the melting of the DNA oligonucleotides. Because of the molecular recognition properties associated with the DNA interconnects, this strategy allows one to control interparticle distance, strength of the particle interconnects, and size and chemical identity of the particles in the targeted macroscopic structure.

In the same time, Alivisatos et al. [9] also reported DNA-based techniques to organize gold nanocrystals into spatially defined structures. In their work, gold particles were attached to either the 3' or 5' end of 19 nucleotide long single-stranded DNA molecules through the well-known thiol attachment scheme. Then, 37 nucleotide long single-stranded DNA template molecules were added to the solution containing the gold nanoparticles functionalized with single-stranded DNA. The authors showed that the nanocrystals could be assembled into dimers (parallel and antiparallel) and trimers upon

hybridization of the DNA molecules with that of the template molecule. Due to the ability to choose the number of nucleotides, the gold particles can be placed at defined positions from each other as schematically shown in Fig. 3.

Based on the work of Alivisatos and co-workers, Loweth et al. [17] have studied further details of the formation of the hetero-dimeric and hetero-trimeric nonperiodic nanocluster molecules. They showed exquisite control of the placement of 5 nm and 10 nm gold nanoclusters that were derivatized with single-stranded DNA. Various schemes of hetero-dimers and hetero-trimers were designed and demonstrated with TEM images [17].

Mucic et al. [18] have made the construction of binary nanoparticle networks composed of 9 nm particles and 31 nm particles, both composed of citrate-stabilized colloidal gold. These 9 and 31 nm particles are coated with different 12-mer oligonucleotides via a thiol bond. When a third DNA sequence (24-mer), which is complementary to the oligonucleotides on both particles is added, hybridization led to the association of particles. When the ratio of 9 nm to 31 nm particles is large, a binary assembly of the nanoparticles is formed. Fig. 4 shows the scheme and a TEM image of the binary nanoparticle assembly [18].

Maeda et al. recently reported two-dimensional assembly of Au nanoparticles with a DNA network template [19]. Fig. 5 illustrates their approach. First, a gold nanoparticle is attached to a DNA1 molecule through the Au-thiol reaction. The DNA1 molecule is then hybridized with a DNA2 molecule possessing a counterbase sequence. Finally, the components are built into a DNA network consisting of DNA3 through the hybridization of DNA2 and DNA3. As a consequence, the Au particles are inserted into the DNA3 network template.

4.3 Construction of semiconductor particle arrays using DNA

Many strategies have been used to synthesize semiconductor particles and particle arrays. Coffer and co-workers were the first to utilize DNA as a stabilizer/template to form both CdS nanoparticles and mesoscopic aggregates from them [20]. Their original efforts were based on the use of linear duplexes of DNA in solution as a stabilizer for forming CdS nanoparticles. The initial results indicated that CdS nanoparticles could be formed from Cd^{2+} and S^{2-} in the presence of DNA. However, the role of DNA in the formation of the nanoparticles and the interactions between DNA and the particles after their formation were not clarified [20]. Further studies demonstrated that DNA base sequence, and more specifically the content of the base adenine, had a significant effect on the size of the CdS particles formed and their resulting photophysical properties [21].

In order to form well-defined mesoscale structures in solution, Coffer and co-workers developed a new strategy for binding a template DNA strand to a solid substrate [22]. This approach provides many possibilities for synthesizing mesoscale structures since particle composition, shape, length, and sequence of the DNA template can be controlled. The main drawback of this approach is the difficulty of forming monodispersed nanoparticle samples since the nature of the DNA/Cd^{2+} interactions is poorly understood. In addition, the relative spacing and orientation of the resulting nanoparticles within the mesostructure are difficult to control, and consequently, tailoring and predicting the resulting properties of the materials is problematic [22].

Torimoto et al. tried another approach to assemble CdS nanoparticle using DNA [23]. The idea is to use the electrostatic interaction between the cationic surface modifiers on the CdS nanoparticles and the phosphate groups in DNA double strands. Fig. 6 shows the schematic illustration of their approach.

Mitchell et al. used thiolated oligonucleotides to partially displace mercaptopropionic acid molecules from the surface of the dots [24]. However, the presence of carboxyl groups on the surface of the nanocrystals was found to cause strong nonspecific binding to the oligonucleotides probe backbone. To overcome this problem, Pathal et al. developed a strategy in which hydroxylated CdSe/ZnS nanocrystals were covalently attached to oligonucleotide sequences via a carbamale linkage [25].

Tour and co-workers taken an approach similar to that of Coffer in using DNA to assemble DNA/fullerene hybrid organic materials [26]. In their strategy, the negative phosphate backbone of DNA was used as a template to bind and organize C_{60} fullerene molecules modified with a N,N-dimethylpyrrolidinium iodide moiety into defined mesoscopic architectures. The modified fullerene is electrostatically complexed to the DNA backbone through cation exchange with sodium in DMSO as depicted in Fig 7.

4.4 DNA-directed nanowires

The concept of DNA-mediated self-assembly of nanostructures has also been extended to metallic nanowires [27-29]. Braun et al. have utilized DNA as a template to grow conducting silver nanowires [27]. The basic assembly scheme for constructing a Ag nanowire attached to two gold electrodes is outlined in Fig 8. Two gold electrodes separated by a defined distance (12-16 μm) were deposited onto a glass slide using photolithography. The gold electrodes subsequently were modified with noncomplementary hexane disulfide modified oligonucleotides through well-established thiol adsorption chemistry on Au. Subsequently, a fluorescently labeled strand of DNA containing sticky ends that are complementary to the oligonucleotides attached to the electrodes is introduced. Hybridization of the fluorescently tagged DNA molecule to the surface-confined alkylthiololigonucleotides was confirmed by fluorescence microscopy, which showed a fluorescent bridge connecting the two electrodes (see Fig. 9). After a single DNA bridge was observed, the excess hybridization reagents were removed. Silver ions then were deposited onto the DNA through cation exchange with sodium and complexation with the DNA bases. This process can be followed by monitoring the quenching of the fluorescent tag on the DNA by the Ag ions. After almost complete quenching of the fluorescence, the silver ion bound to the template DNA is reduced using standard hydroquinone reduction procedures to form small silver aggregates along the backbone of the DNA. A continuous silver wire is then formed by further Ag ion deposition onto the previously constructed silver aggregates followed by reduction. The wires are comprised of 30-50 nm Ag grains that are contiguous along the DNA backbone. Two terminal electrical measurements subsequently were performed on the Ag wire depicted in the AFM image. When the current-voltage characteristics of the Ag wire were monitored, no current was observed at near zero bias (10 V in either scan direction), indicating an extremely high resistance. At a higher bias, the wire becomes conductive. Surprisingly, the current-voltage characteristics were dependent on the direction of the scan rate, yielding different I-V curves. Although not well understood, it was postulated that the individual Ag grains that comprise the Ag nanowires may require simultaneous

charging, or Ag corrosion may have occurred, resulting in the high resistance observed at low bias. By depositing more silver and thereby growing a thicker Ag nanowire, the no-current region was reduced from 10 V to 0.5 V, demonstrating crude control over the electrical properties of these systems. In addition, control experiments where one of the components (DNA or Ag) was removed from the assembly produced no current, establishing that all of the components are necessary to form the conducting Ag nanowires. This work is a proof-of-concept demonstration of how DNA can be used in a new type of chemical lithography to guide the formation of nanocircuitry.

Martin et al. also reported the fabrication of Au and Ag wires using the DNA as a template or skeleton [28]. The basic idea behind this work is to fabricate gold or platinum metal wires, functionalize these wires with exchange and formation of complexes between the gold and the DNA bases. Current voltage characteristics were measured to demonstrate the possible use of these nanowires. The authors also reported the formation of luminescent self-assembled poly (p-phenylene vinylene) wires for possible optical applications [29]. The work has a lot of potential and much room for further research to control the wire width, the contact resistances between the gold electrode and the silver wires, and use of other metals and materials.

More recently, Yan et al. [30] demonstrated the design and construction of a DNA nanostructure that has a square aspect ratio and readily self-assembles into two distinct lattice forms: nanoribbons and two-dimensional nanogrids. The 4 × 4 tile contains four four-arm DNA branched junctions pointing in four directions. Such nanogrids have a large cavity size, which may serve as binding or tethering sites for other molecular components. For example, the loops at the center of each 4 × 4 tile can be modified with appropriate functional groups and for used as a scaffold for directing periodic assembly of desired molecules. Periodic protein arrays were achieved by templated self-assembly of streptavidin onto the DNA nanogrids. The authors also used the 4 × 4 tile assemblies as templates to construct a highly conductive, uniform-width silver nanowire. A two-terminal I-V measurement of the resulting silver nanowire was conducted at room temperature. The I-V curve is linear, demonstrating Ohmic behavior in the range of – 0.2 to 0.2 V. This nanowire is easily reproducible and has markedly higher conductivity than previously reported double-helix DNA-templated silver nanowires [27].

In addition to using DNA, there are also reports on using other biomolecules to fabricate nanowires. Djalali et al. recently developed a new biological approach to fabricate Au nanowires using sequenced peptide nanotubes as templates [31]. The fabrication process is illustrated in Fig. 10. Briefly, Au ions are captured by imidazole and amine groups of the sequenced peptides on the nanotubes, and then the trapped Au ions in the peptides nucleate into Au nanocrystals after reducing those ions by hydrazine hydrate. This approach has potential to control the size and the packing density of the Au nanocrystals by simply adjusting external experimental conditions such as pH, temperature, and ion concentration.

4.5 DNA functionalized with carbon nanotubes

Single-walled carbon nanotubes (SWNT) are composed of a single layer of graphene sheet rolled-up into a cylinder, with diameters in the range 1-2 nm [32-34]. Fig. 11 shows a TEM image of a single-walled carbon nanotube. Since the discovery of single-walled carbon nanotubes [33-35], this new class of materials has demonstrated great potential to

make a major contribution to a variety of nanotechnology applications, including molecular electronics [36], hydrogen storage media [37], and scanning probe microscope tips [38]. Carbon nanotubes can be expected to provide a basis for a future generation of nanoscale devices, and it has been predicted that modification of SWNT will lead to an even more diverse range of applications. For example, the electrical properties of empty SWNT are extremely sensitive to their structure and the existence of defects, which imposes great difficulty for using unfilled nanotubes in electronic device applications. The property of filled SWNT, on the other hand, will be dominated by the filling materials, and therefore, filled nanotubes will be more robust in applications such as nanoelectronics [39-41]. The unusual physical and chemical properties also depend on the nanotube diameter and helicity. Kiang and co-workers developed an efficient method for catalytic synthesis of SWNTs with a wide range of diameters [42, 43]. Many applications would benefit from the availability of SWNT of varying diameters and helicities.

At present, SWNT-based devices are fabricated by "top-down" lithographic methods. The construction of more complex architectures with high device density requires the development of a "bottom-up," massively parallel strategy that exploits the molecular properties of SWNTs. DNA-guided assembly of carbon nanotubes could be one way toward this aim. Besides, carbon nanotubes have useful properties for various potential applications in biological devices. For instance, nanotubes can be used as electrodes for detecting biomolecules in solutions, similar to commonly used conventional carbon based electrode materials. Also, the electrical properties of SWNTs are sensitive to surface charge transfer and changes in the surrounding electrostatic environment, undergoing drastic changes simply by adsorption of certain molecules or polymers. SWNTs are therefore promising as chemical sensors for detecting molecules in the gas phase and as biosensors for probing biological processes in solutions.

One way to link DNA with nanotubes is via noncovalent interactions [44-47]. Dai and co-workers described a simple and general approach to noncovalent functionalization of the sidewalls of SWNTs and subsequent immobilization of various biological molecules onto nanotubes with a high degree of control and specificity [46]. Their method involves a bifunctional molecule, 1-pyrenebutanoic acid, succinimidyl ester, irreversibly adsorbed onto the inherently hydrophobic surfaces of SWNTs in an organic solvent dimethylformamide (DMF) or methanol. The pyrenyl group, being highly aromatic in nature, is known to interact strongly with the basal plane of graphite via π-stacking, and also found to strongly interact with the sidewalls of SWNTs in a similar manner, thus providing a fixation point for the biomolecule on the nanotubes. The anchored molecules on SWNTs are highly stable against desorption in aqueous solutions. This leads to the functionalization of SWNTs with succinimidyl ester groups that are highly reactive to nucleophilic substitution by primary and secondary amines that exist in abundance on the surface of most proteins (Fig. 12). The mechanism of protein immobilization on nanotubes, then, involves the nucleophilic substitution of N-hydroxysuccinimide by an amine group on the protein, resulting in the formation of an amide bond. This technique enables the immobilization of a wide range of biomolecules on the sidewalls of SWNTs with high specificity and efficiency.

Meanwhile, people also tried to use covalent chemistry to link DNA with nanotubes because covalent interaction is expected to provide the best stability, accessibility, and

selectivity during competitive hybridization. Hamers and co-workers have developed a multi-step route to the formation of covalently linked adducts of SWNT and DNA oligonucleotides [48]. Figure 13 shows an overview of the covalent attachment process. Purified SWNTs were oxidized to form carboxylic acid groups at the ends and sidewalls. These were reacted with thionyl chloride and then ethylenediamine to produce amine-terminated sites. The amines were then reacted with the heterobifunctional cross-linker succinimidyl 4-(N-maleimidomethyl)cyclohexane-1-carboxylate, (SMCC), leaving the surface terminated with maleimide groups. Finally, thiol-terminated DNA was reacted with these groups to produce DNA-modified SWNTs. It is found that DNA molecules covalently linked to SWNTs are accessible to hybridization as evidenced by strong tendency in hybridization with molecules having complementary sequences compared with noncomplementary sequences.

Williams et al. [49] recently developed a way to couple SWNTs covalently to peptide nucleic acid (PNA, an uncharged DNA analogue [50]) and to hybridize these macromolecular wires with complementary DNA. This technique is shown in Fig. 14. It is found that DNA attachment occurs predominantly at or near the nanotube ends. Dwyer et al. also reported some progress toward the DNA-guided assembly of carbon nanotubes [51]. They used amine-terminated DNA strands to functionalize the open ends and defect sites of single-walled carbon nanotubes. Fig. 15 illustrates the DNA/nanotube reaction scheme. Nguyen et al. developed an approach for the attachment of DNA to oxidatively opened ends of multiwalled carbon nanotube arrays [52]. In addition to necessary steps such as opening the closed carbon nanotube (CNT) ends and removing metal catalyst at the nanotube tips, a novel and critical step in their approach is the deposition of a spin-on glass (SOG) film inside hydrophobic CNT arrays. It is found that the SOG improves the mechanical rigidity of the CNT array as well as enhances the DNA coupling efficiency.

In addition to DNA, there are also plenty of interests in functionalizing carbon nanotubes with other biomolecules such as protein, peptide, etc. Pantarotto et al. recently reported the synthesis, structural characterization, and immunological properties of carbon nanotubes functionalized with peptides [53]. They employed two different methods (Fig. 16) to link bioactive peptides to SWNTs through a stable bond: (i) the fragment condensation of fully protected peptides and (ii) selective chemical ligation.

4.6 Field effect transistor based on DNA

Mrauccio et al. [54] have demonstrated a field effect transistor based on a deoxyguanosine derivative (a DNA base). This three-terminal field effect nanodevice was fabricated starting from a deoxyguanosine derivative ($dG(C_{10})_2$). Guanosine has been chosen because of its peculiar sequence of H-bond donor or acceptor groups, and because it has the lowest oxidation potential among the DNA bases, which favors self-assembly and carrier transport, respectively. Such a guanosine supramolecular assembly has the form of long ribbons (see Figure 17), with a strong intrinsic dipole moment along the ribbon axis that causes current rectification in transport experiments. The prototype structure of this nanodevice is a planar metal-insulator-metal nanojunction, consisting of two arrow-shaped metallic electrodes facing each other and connected by the supramolecular structures. A third electrode (gate) is deposited on the back of the device to produce a field effect transistor (see Figure 17). The experiments on transport through the source and drain electrodes interconnected by self-assembled guanine ribbons suggest

that these devices behave like p-channel MOSFETs. The devices exhibit a maximum voltage gain of 0.76. This prototype transistor represents a starting point toward the development of biomolecular electronic devices. In particular, the demonstration of a three-terminal field effect device (field effect transistor) consisting of source and drain contacts interconnected by a molecular layer, and a third contact (gate) to modulate the drain-source current (Ids), is a crucial step for the development of a molecular electronics road map.

4.7 Self-assembly using artificial DNA

Among the variety of approaches to DNA-based supramolecular chemistry, the strategy of replacing DNA natural bases by alternative bases that possess distinct shape, size, or function has allowed the modification of DNA in a highly specific and site-selective manner [55-59]. One good example is the replacement of the natural bases by artificial nucleosides or nucleoside mimics [56]. However, this approach is restricted to molecules with shapes and sizes that are commensurate to normal bases to ensure that the DNA modifications occur highly specifically and site selectively [56]. Recently, a new generation of such nucleoside mimics was reported in which the hydrogen bonding interactions were replaced by metal-mediated base pairing [60-64]. The advantage of this modification strategy is that it allows the metal ions to be replaced in the interior of the DNA duplex. This represents an important structural prerequisite for the development of new molecular devices based on interacting metal centers. Metal ions such as Cu^{2+}, Pd^{2+}, and Ag^{+}, have been successfully incorporated as artificial DNA bases into oligonucleotides by different groups (Fig. 18) [58]. Introduction of such metal-induced base pairs into DNA would not only affect the assembly-disassembly processes and the structure of DNA double strands but also confer a variety of metal-based functions upon DNA. A remarkable consequence of the insertion of just one artificial metal-ion-mediated base pair is that the thermal stability of the modified DNA duplex is strongly enhanced relative to one with normal hydrogen-bond interactions.

Tanaka et al. [60] showed that replacement of hydrogen-boned base pairing present in natural DNA by metal-mediated base pairing, with the subsequent arrangement of these metallo-base pairs into a direct stacked contact, could lead to "metallo-DNA" in which metal ions are lined up along the helix axis in a controlled and stepwise manner. Later, they successfully arranged Cu^{2+} ions into a magnetic chain using the artificial DNA [65]. Fig. 19 shows the schematic representation of Cu-mediated duplex formation between two artificial DNA strands in which hydroxypyridone nucleobases replace natural base pairs. The most important structural feature of this artificial DNA is the alignment of the Cu^{2+} ions along the axes inside the duplexes. The canonical helical conformation of these DNA-like duplexes ensures regular Cu^{2+}-Cu^{2+} distances. From EPR signals the distance in the artificial DNA duplexes was estimated to be 3.7 Å, which is remarkably similar to the distance between two adjacent base pairs in natural DNA duplexes (3.4 Å).

5. DNA-based nanomaterials as biosensors

In recent years, there have been significant interests in using novel solid-state nanomaterials for biological and medical applications. The unique physical properties of nanoscale solids (dots or wires) in conjunction with the remarkable recognition

capabilities of biomolecules could lead to miniature biological electronics and optical devices including probes and sensors. Such devices may exhibit advantages over existing technology not only in size but also in performance. In this section, we describe some good examples that utilize nanostructured materials conjugated with biomolecules as novel biosensors.

Sequence-specific DNA detection is an important topic because of its application in the disgnosis of pathogenic and genetic diseases. Many detection techniques have been developed that rely upon target hybridization with radioactive, fluorescent, chemiluminescent, or other types of labeled probes. Moreover, there are indirect detection methods that rely on enzymes to generate colorimetric, fluorescent, or chemiluminescent signals. Mirkin and co-workers [66, 67] developed a novel method for detecting polynucleotides using gold nanoparticle probes. Their method utilizes the distance- and size-dependent optical properties of aggregated Au nanoparticles functionalized with 5'-(alkanethiol)-capped oligonucleotides. Introduction of a single-stranded target oligonucleotide (30 bases) into a solution containing the appropriate probes resulted in the formation of a polymeric network of nanoparticles with a concomitant red-to-pinkish/purple color change. Hybridization was facilitated by annealing and melting of the solutions, and the denaturation of these hybrid materials showed transition temperatures over a narrow range that allowed differentiation of a variety of imperfect targets. Transfer of the hybridization mixture to a reverse-phase silica plate resulted in a blue color upon drying that could be detected visually. The unoptimized system can detect about 10 femtomoles of an oligonucleotide. This method has many desirable features including rapid detection, a colorimetric response, good selectivity, and a little or no required instrumentation. Later, the same group reported a related method in which the Au nanoparticles functionalized with 5'- and 3'-(alkanethiol)-capped oligonucletides that causes a tail-to-tail alignment of Au nanoparticle probes [67]. This new system exhibits extraordinary selectivity and provides a simple means for colorimetric, one-pot detection of a target oligonucleotide in the presence of a mixture of oligonucleotides with sequences differing by a single nucleotide.

Maxwell et al. [68] also reported that biomolecules and nanoparticles can be both structurally and functionally linked to create a new class of nanobiosensors that is able to recognize and detect specific DNA sequences and single-base mutations in a homogeneous format. The principle of this detection method is illuminated in Fig. 20. At the core of this biosensor is a 2.5 nm gold nanoparticle that functions as both a nano-scaffold and a nano-quencher. Oligonucleotide molecules labeled with a thiol group are attached at one end of the core and a fluorophore at the other end. This hybrid construct is found to spontaneously assemble into a constrained arch-like conformation on the particle surface. In the assembled state, the fluorophore is quenched by the nanoparticle. Upon target binding, the constrained conformation opens and the fluorophore leaves the surface because of the structural rigidity of the hybridized DNA (double-stranded), and fluorescence is restored. This structural change generates a fluorescence signal that is highly sensitive and specific to the target DNA.

Cao et al. [69] have also developed a nanoparticle-based method for DNA and RNA detection in which Au nanoparticle probes are labeled with oligonucleotides and Raman-active dyes. The scheme of their method is shown in Fig. 21. The gold particles form a template for silver reduction, and the silver coating acts as a surface-enhanced Raman

scattering promoter for the dye-labeled particles that have been captured by target molecules and an underlying chip in microarray format. Compared with fluorescence-based chip detection, this nanoparticle-based methodology offers several advantages. The ratio of Raman intensities can be extracted from a single Raman spectrum with single-laser excitation. Second, the number of available Raman dyes is much greater than the number of available and discernable fluorescent dyes. Therefore, this method offers potentially greater flexibility, a larger pool of available and nonoverlapping probes, and higher multiplexing capabilities than do conventional fluorescence-based detection approaches.

A major challenge in the area of DNA detection is the development of methods that do not rely on polymerase chain reaction or comparable target-amplification systems that require additional instrumentation and reagents. Park et al. [70] reported an electrical method for DNA detection. They find that the binding of oligonucleotides functionalized with gold nanoparticles leads to conductivity changes associated with target-probe binding events. The binding events localize gold nanoparticles in an electrode gap; silver deposition facilitated by these nanoparticles bridges the gap and leads to readily measurable conductivity changes. With this method, they have detected target DNA at concentration as low as 500 femtomolar with a point mutation selectivity factor of ~ 100,000:1.

Wang et al. [71] reported a nanoparticle-based protocol for detecting DNA hybridization. The idea is based on a magnetically induced solid-state electrochemical stripping detection of metal tags. Their approach involves the hybridization of a target oligonucleotide to probe-coated magnetic beads, followed by binding of the streptavidin-coated gold nanoparticles to the captured target, catalytic silver precipitation on the gold particle tags, a magnetic collection of the DNA-linked particle assembly and solid-state stripping detection. The DNA hybrid bridges the metal nanoparticles to the magnetic beads, with multiple duplex links per particle. Most of the three-dimensional DNA-linked aggregate is covered with silver following the catalytic precipitation of silver on gold. Such DNA-linked particle assembly can thus be collected magnetically and anchored onto the thick-film working electrode. This leads to a direct contact of the silver with the surface and enables the solid-state electrochemical transduction.

Weizmann et al. also emploied nucleic acid-functionalized magnetic particles for amplified DNA sensing and immunosensing [72]. Fig. 22 outlines the concept for the amplified detection of a target DNA 2. Amine-functionalized borosilicate-based magnetic particles were modified with DNA 1 using the heteronifunctional corss-linker 3-maleimidopropionic acid N-hydroxysuccinimide ester. The probe 1 is complementary to a part of the target sequence 2. The 1-functionalized magnetic particles are hybridized in a single step with a mixture that includes the target 2 and the biotin-labeled nucleic acid 3 that is complementary to the free segment of 2. The three-component double-stranded DNA assembly is then interacted with avidin-horseradish peroxidase (HRP) that act as a biocatalytic label. The DNA/avidin-HPR-functionalized magnetic particles are subsequently mixed with magnetic particles modified with the naphthoquinone unit 4. The mixture of the magnetic particles is then attracted to the electrode supported by means of an external magnet. Electrochemical reduction of the naphthoquinone to the respective hydroquinone results in the catalyzed reduction of O_2 to H_2O_2. The electrogenerated H_2O_2 leads, in the presence of luminal 5 and the enzyme label HRP, to

the generation of the chemiluminescence signal. The chemiluminescence occurs only when the target DNA 2 is in the analyzed sample. Furthermore, the light intensity relates directly to the number of recognition pairs of 1 and 2 associated with the electrode, and thus it provides a quantitative measure of the concentration of 2 in the sample. The subsequent rotation of the particles on the surface by means of the rotating external magnet results in the enhanced electrogenerated chemiluminescence, because the magnetic particle behave as rotating microelectrode, where the interaction of O_2 and luminal with the catalysts on the electrode is controlled by convection rather than by diffusion. Thus, the rotation of the magnetic particles yields amplified detection of DNA.

He et al. [73] recently described a new approach for ultrasensitive detection of DNA hybridization based on nanoparticle-amplified surface plasmon resonance (SPR). Use of the Au nanoparticle tags leads to a greater than 10-fold increase in angle shift, which corresponds to a more than 1000-fold improvement in sensitivity for the target oligonucleotide as compared to the unamplified binding event. This enhanced shift in SPR reflectivity is a combined result of greatly increased surface mass, high dielectric constant of Au particles, and electromagnetic coupling between Au nanoparticles and the Au film. DNA melting and digestion experiments further supported the feasibility of this approach in DNA hybridization studies. The extremely large angle shifts observed in particle-amplified SPR make it possible to conduct SPR imaging experiments on DNA arrays. The sensitivity of this technique begins to approach that of traditional fluorescence-based methods for DNA hybridization. These results illustrate the potential of particle-amplified SPR for array-based DNA analysis and ultrasensitive detection of oligonucleotides.

Su et al. [74] demonstrated a microcantilever based mechanical resonance DNA detection using gold nanoparticle-modified probes. The core idea is to measure the mass change of a microfabricated cantilever induced by DNA hybridization through the shift of the resonance frequency of the cantilever. The hybridization is reflected by the attachment of gold nanoparticles on the cantilever and then chemically amplified by gold nanoparticle-catalyzed nucleation of silver in a developing solution. The authors claim that this method can detect target DNA at a concentration of 0.05 nM or lower. When combined with stringent washing, this technique can detect a single base pair mismatched DNA strand. The cantilever is 1/100 times smaller than its macroscopic quartz crystal microbalance counterpart, and it can be mass-produced as miniaturized sensor arrays by current processing technology. Multiple DNA detection is also possible by coating multiple cantilevers with various capture DNA strands and monitoring the change in their resonance frequencies.

Nanoparticle-based biosensors can also be used for the physical and chemical manipulation of biological systems. Hamad-Schifferli et al. [75] recently demonstrated remote control of the hybridization behavior of DNA molecules by inductive coupling of a radio-frequency magnetic field to a Au nanocrystal covalently linked to DNA. When the magnetic field is on, the inductive coupling to the Au nanocrystal increases the local temperature of the bound DNA, thereby inducing denaturation while leaving surrounding molecules relatively unaffected. Removing the field restores the hybridization of DNA. Because dissolved biomocelues dissipate heat in less than 50 picoseconds, the switch is fully reversible. This concept shows promising potential for the control of hybridization and other biological functions on the molecular scale.

There are also intense studies on semiconductor quantum dots conjugated with biomolecules as novel probes [76-78]. These nanometer-sized conjugates are water-soluble and biocompatible, and provide important advantages over organic dyes and lanthanide probes. In particular, the emission wavelength of quantum-dot nanocrystals can be continuously tuned by changing the particle size, and a single light source can be used for simultaneous excitation of all different-sized dots. High-quality dots are also highly stable against photobleaching and have narrow, symmetric emission spectra. These novel optical properties render quantum dots ideal fluorophores for ultrasensitive, multicolor, and multiplexing applications in molecular biotechnology and bioengineering.

6. Properties of DNA-linked gold nanoparticles

The DNA-linked gold nanoparticle assembly is a prototype of DNA-based nanostructures. The optical and melting properties of this system have attracted considerable interest because the understanding of these properties is essential for DNA-based nanotechnology [79-81]. As described in section 4, the preparation of DNA-linked gold nanoparticles involves two batches of gold particles that are functionalized with noncomplementary DNA oligonucleotides with sequences **a** and **b**, respectively. When another oligonucleotide (linker) with a complementary sequence **a'b'** is introduced, the gold nanoparticles self-assemble into aggregates. In this section, we describe the optical and melting properties of such DNA-linked gold nanoparticle assemblies.

6.1 Aggregation of DNA-modified gold nanoparticles

UV-visible absorption spectroscopy is a suitable tool to study the optical properties of DNA-linked gold nanoparticle aggregation because DNA bases and gold nanoparticles have strong absorption in the UV region (~ 260 nm) and the visible light region (~ 520 nm), respectively. The extinction coefficient of a collection of gold particles is sensitive to the size of the aggregates. Thus, the change in the gold extinction reflects the aggregation of the gold nanoparticles. The kinetics of aggregation of DNA-linked gold nanoparticles is studied by measuring the UV-visible spectrum as a function of time at room temperature, as illustrated in Fig. 23 [81]. Upon adding linker DNA, the DNA hybridization leads to aggregation of gold nanoparticles, as demonstrated in the gold surface plasmon peak (520 nm) shift of the DNA-modified gold nanoparticles [82, 83]. The aggregation starts with the wavelength shift of the plasmon band, followed by broadening and more shifting of the peak as hybridization continues. These results indicate that the initial aggregation takes place with increasing volume fraction, followed by increasing network size [84, 85].

6.2 Melting of DNA-linked gold nanoparticle aggregations

The UV-visible spectrum is also used to monitor the melting properties of the DNA-linked aggregates. The DNA double helix has a smaller extinction coefficient than does single-stranded DNA due to hypocromism, and, therefore, the absorption intensity at 260 nm increases as a result of DNA melting. Meanwhile, the melting will also cause sharp changes in the gold nanoparticle extinction coefficient due to the dissociation of the aggregate. Therefore, the melting can be monitored at either 260 nm or 520 nm as a function of temperature. The 260 and 520 nm melting curves are very similar, indicating

that DNA and gold nanoparticle melting are closely correlated. Fig. 24 displays the melting curves of 10, 20, and 40 nm gold particles with linker DNA [81]. The melting transition width is about 5 K, compared to 12 K for melting of free DNA. The transition width as well as the melting temperature has been dramatically modified by the binding to gold particles. It is also clear that the melting properties are highly dependent on the gold nanoparticle size. For bigger gold particles the melting temperature is higher [81, 85].

6.3 Effects of external variables on the melting properties

Besides the particle size, the melting properties of DNA-linked gold nanoparticles are also strongly dependent on other variables, including the DNA density on the gold surface, the interparticle distance, and the salt concentration in the solution. Jin et al. recently performed a series of experiments to systematically study the effects of various external variables [80].

A high DNA surface density on the Au nanoparticle is expected to provide advantage in particle stabilization as well as to increase the hybridization efficiency. Experimental results show that for temperature below 70 °C, the melting temperature is proportional to the DNA surface density when the nanoparticle and target concentrations are kept constant [80]. Also, a slight broadening of the melting transition was observed as the DNA density decreases.

The interparticle distance is another key parameter to control the melting properties. As gold nanoparticles are linked together via DNA hybridization, electromagnetic coupling between the nanoparticles result in significant damping of their surface plasmon resonances. The amount of extinction due to scattering is also influenced by the interparticle spacing. Interparticle distance also influences van der Waals and electrostatic forces between the particles, weakly affecting duplex DNA stability and hybridization/dehybridization properties. Experimental results show that the melting temperature increases with the length of the interparticle distance for temperatures below 70 °C, and there is a linear relationship between the two [80].

The melting behavior of DNA-linked nanoparticle aggregation also depends on the salt concentration. In Jin et al's study [80], the melting temperature increased from 41 to 61.5 °C as the salt concentration was increased from 0.05 to 1.0 M while keeping the nanoparticle and linker DNA concentration constant. Moreover, increasing salt concentration also causes larger aggregates as evidenced by a larger absorption change during melting. It is believed that the salt brings about a screening effect that minimizes electrostatic repulsion between the DNA-DNA bases and between the nanoparticles, hence, strengthening the effect of the linker bond.

7. Conclusion

Due to its unique recognition capabilities, physicochemical stability, mechanical rigidity, and high precision processibility, DNA is a promising material for "biomolecular nanotechnology." The study of DNA-based nanostructures is hence an attractive topic. This review describes the utilization of DNA for preparing nanostructured materials and use of such nanostructures for biological and medical applications. Various DNA-based nanostructures, including nanostructures by DNA itself, DNA functionalized with metal

and semiconductor nanoparticles, DNA-directed nanowires, and DNA-functionalized carbon nanotubes, were described. Some good examples of using DNA-based nanostructures as biosensor are also presented.

Though significant progress has been made, the study of DNA-based nanostructures is still at its early stage. The catalytic, electrical, magnetic, and electrochemical properties of such structures have not yet been systematically investigated, and they, therefore, represent new frontiers in this field. It is anticipated that new phenomena and useful structures will continue to emerge over the next few years. Advanced study in this field will not only provide valuable fundamental information about the collective physical and chemical properties of nanoparticles and DNA, but also may provide access to new and useful electronic and photonic materials applicable to the industry.

References

1. R. G. Nuzzo and D. L. Allara, J. Am. Chem. Soc. 105, 4481 (1983).
2. L. H. Dubois and R. G. Nuzzo, Annu. Rev. Phys. Chem. 43, 437 (1992).
3. T. M. Herne and M. J. Tarlov, J. Am. Chem. Soc. 119, 3401 (1997).
4. M. Yang, H. C. M. Yau, and H. L. Chan, Langmuir 14, 6121 (1998).
5. C. D. Bain and G. M. Whitesides, Agnew. Chem. Int. Ed. Engl. 28, 506 (1989); C. D. Bain, E. B. Troughton, Y. T. Tao, J. Evall, G. M. Whitesides, and R. G. Nuzzo, J. Am. Chem. Soc. 111, 321 (1989).
6. J. J. Hickman, P. E. Laibinis, D. I. Auerbach, C. Zou, T. J. Gardner, G. M. Whitesides, and M. S. Wrighton, Langmuir 8, 357 (1992).
7. T. M. Herne and M. J. Tarlov, J. Am. Chem. Soc. 119, 3401 (1997).
8. S. Pathak, S. K. Choi, N. Arnheim, and M. E. Thompson, J. Am. Chem. Soc. 123, 4103 (2001).
9. A. P. Alivisatos, K. P. Johnsson, X. Peng, T. E. Wilson, C. J. Loweth, M. P. Bruchez, and P. G. Schultz, Nature 382, 609 (1996).
10. C. M. Niemeyer, W. Burger, and J. Peplies, Angew. Chem. Int. Ed. 37, 2265 (1998).
11. N. C. Seeman, J. Theor. Biol. 99, 237 (1982).
12. N. C. Seeman, Nanotechnology 2, 149 (1991).
13. E. Winfree, F. Liu, L. Wenzler, and N. C. Seeman, Nature 394, 539 (1998).
14. N. C. Seeman, Annu. Rev. Biophys. Biomol. Struct. 27, 225 (1998).
15. J. Shi and D. E. Bergstrom, Angew. Chem., Int. Ed. Engl. 36, 111 (1997).
16. C. A. Mirkin, R. L. Letsinger, R. C. Mucic, and J. J. Storhoff, Nature 382, 607 (1996).
17. C. J. Loweth, W. B. Caldwell, X. Peng, A. P. Alivisatos, and P. G. Schultz, Agnew. Chem. Int. Ed. 38, 1808 (1999).
18. R. C. Mucic, J. J. Storhoff, C. A. Mirkin, and R. L. Letsinger, J. Am. Chem. Soc. 120, 12674 (1998).
19. Y. Maeda, H. Tabata, and T. Kawai, Appl. Phys. Lett. 79, 1181 (2001).
20. J. L. Coffer, S. R. Bigham, R. F. Pinizzotto, and H. Yang, Nanotechnology 3, 69 (1992).
21. S. R. Bigham and J. L. Coffer, Colloids Surfaces A 95, 211 (1995).
22. J. L. Coffer, S. R. Bigham, X. Li, R. F. Pinizzotto, Y. G. Rho, R. M. Pirtle, and I. L. Pirtle, Appl. Phys. Lett. 69, 3851 (1996).

23. T. Torimoto, M. Yamashita, S. Kuwabata, T. Sakata, H. Mori, and H. Yoneyama, J. Phys. Chem. B, 103, 42 (1999).
24. G. P. Mitchell, C. A. Mirkin, and R. L. Letsinger, J. Am. Chem. Soc. 121, 8122 (1999).
25. S. Pathak, S.-K. Choi, N. Arnheim, and M. E. Thompson, J. Am. Chem. Soc. 123, 4103 (2001).
26. A. M. Cassell, W. A. Scrivens, and J. M. Tour, Angew. Chem., Int. Ed. Engl. 37, 1528 (1998).
27. E. Braun, Y. Eichen, U. Sivan, and G. Ben-Yoseph, Nature 391, 775 (1998).
28. B. R. Martin, D. J. Dermody, B. D. Reiss, M. Fang, L. A. Lyon, M. J. Natan, and T. E. Mallouk, Adv. Mater. 11, 1021 (1999).
29. T. S. Mayer, T. N. Jackson, M. J. Natan, and T. E. Mallouk, 1999 Materials Research Society Fall Meeting Digest (1999) p. 157.
30. H. Yan, S. H. Park, G. Finkelstein, J. H. Reif, and T. H. Labean, Science 301, 1882 (2003).
31. R. Djalali, Y. Chen, and H. Matsui, J. Am. Chem. Soc. 125, 5873 (2003).
32. S. Iijima, Nature 354, 56 (1991).
33. S. Iijima and T. Ichihashi, Nature 363, 603 (1993).
34. D. S. Bethune, C.-H. Kiang, M. S. de Vries, G. Gorman, R. Savoy, J. Vazquez, and R. Beyers, Nature 363, 605 (1993).
35. C.-H. Kiang and W. A. Goddard III, Phys. Rev. Lett. 76, 2515 (1996).
36. S. J. Tans, A. R. M. Verschueren, and C. Dekker, Nature 393, 49 (1998).
37. A. C. Dillon, K. M. Jones, T. A. Bekkedahl, C.-H. Kiang, D. S. Bethune, and M. J. Heben, Nature 386, 377 (1997).
38. S. S. Wong, E. Joselevich, A. T. Woolley, C. L. Cheung, and C. M. Lieber, Nature 394, 52 (1998).
39. P. M. Ajayan and S. Iijima, Nature 361, 333 (1993).
40. S. C. Tsang, Y. K. Chen, P. J. F. Harris, and M. L. H. Green, Nature 372, 159 (1994).
41. C.-H. Kiang, J.-S. Choi, T. T. Tran, and A. D. Bacher, J. Phys. Chem. B 103, 7449 (1999).
42. C.-H. Kiang, W. A. Goddard III, R. Beyers, J. R. Salem, and D. S. Bethune, J. Phys. Chem. 98, 6612 (1994).
43. C.-H. Kiang, J. Phys. Chem. A 104, 2454 (2000).
44. S. C. Tsang, Z. Guo, Y. K. Chen, M. L. H. Green, H. A. O. Hill, T. W. Hambley, and P. J. Sadler, Angew. Chem., Int. Ed. Engl. 36, 22198 (1998).
45. Z. Guo, P. J. Sadler, and S. C. Tsang, Adv. Mater. 10, 701 (1998).
46. R. J. Chen, Y. Zhang, D. Wang, and H. Dai, J. Am. Chem. Soc. 123, 3838 (2001).
47. M. Shim, N. W. S. Kam, R. J. Chen, Y. Li., and H. Dai, Nano. Lett. 2, 285 (2002).
48. S. E. Baker, W. Cai, T. L. Lasseter, K. P. Weidkamp, and R. J. Hamers, Nano Lett. 2, 1413 (2002).
49. K. A. Williams, P. T. M. Veenhuizen, B. G. de la Torre, R. Eritja, and G. Dekker, Nature 420, 761 (2002).
50. P. E. Nielsen, M. Engholm, R. H. Berg, and O. Buchardt, Science 254, 1497 (1991).

51. C. Dwyer, M. Guthold, M. Falvo, S. Washburn, R. Superfine, and D. Erie, Nanotechnology, 13, 601 (2002).
52. C. V. Nguyen, L. Delzeit, A. M. Cassell, J. Li, J. Han, and M. Meyyappan, Nano Lett. 2, 1079 (2002).
53. D. Pantarotto, C. D. Partidos, R. Graff, J. Hoebeke, J. Briand, M. Prato, and A. Bianco, J. Am. Chem. Soc. 125, 6160 (2003).
54. G. Maruccio, P. Visconti, V. Arima, S. D'Amico, A. Biasco, Eliana D'Amone, R. Cingolani, R. Rinaldi, S. Masiero, T. Giorgi, and G. Gottarelli, Nano Lett. 3, 479 (2003).
55. D. E. Bergstrom, in Current Protocols in Nucleic Acid Chemistry, S. L. Beaucage, D. E. Bergstrom, G. D. Glick, and R. A. Jones, Eds. (Wiley, New York, 2001).
56. E. T. Kool, Acc. Chem. Res. 35, 936 (2002).
57. D.-L. Popescu, T. J. Parolin, and C. Achim, J. Am. Chem. Soc. 125, 6354 (2003).
58. H.-A. Wagenknecht, Angew. Chem. Int. Ed. 42, 3204 (2003).
59. T. Carell, C. Behrens, and J. Gierlich, Org. Biomol. Chem. 1, 2221 (2003).
60. K. Tanaka and M. Shionoya, J. Org. Chem. 64, 5002 (1999).
61. K. Tanaka, Y. Yamada, and M. Shionoya, J. Am. Chem. Soc. 124, 8802 (2002).
62. E. Meggers, P. L. Holland, W. B. Tolman, F. E. Romesber, and P. G. Schultz, J. Am. Chem. Soc. 122, 10714 (2000).
63. H. Weizman and Y. Tor, J. Am. Chem. Soc. 123, 3375 (2001).
64. S. Atwell, E. Meggers, G. Spraggon, and P. G. Schultz, J. Am. Chem. Soc. 123, 12364 (2001).
65. K. Tanaka, A. Tengeiji, T. Kato, N. Toyama, and M. Shionoya, Science 299, 1212 (2003).
66. R. Elghanian, J. J. Storhoff, R. C. Mucic, R. L. Letsinger, and C. A. Mirkin, Science 277, 1078 (1997).
67. J. J. Storhoff, R. Elghanian, R. C. Mucic, C. A. Mirkin, and R. L. Letsinger, J. Am. Chem. Soc. 120, 1959 (1998).
68. D. J. Maxwell, J. R. Taylor, and S. Nie, J. Am. Chem. Soc. 124, 9606 (2002).
69. Y. Cao, R. Jin, and C. A. Mirkin, Science 297, 1536 (2002).
70. S. Park, T. A. Taton, and C. A. Mirkin, Science 295, 1503 (2002).
71. J. Wang, D. Xu, and R. Polsky, J. Am. Chem. Soc. 124, 4208 (2002).
72. Y. Weizmann, F. Patolsky, E. Katz, and I. Willner, J. Am. Chem. Soc. 125, 3452 (2003).
73. Lin He, M. D. Musick, S. R. Nicewarner, F. G. Salinas, S. J. Benkovic, M. J. Natan, and C. D. Keating, J. Am. Chem. Soc. 122, 9071 (2000).
74. M. Su, S. Li, and V. P. Dravid, Appl. Phys. Lett. 82, 3562 (2003).
75. K. Hamad-Schifferli, J. J. Schwartz, A. T. Santos, S. Zhang, and J. M. Jacobson, Nature 415, 152 (2002).
76. W. C. W. Chan, D. J. Maxwell, X. Gao, R. E. Bailey, M. Han, and S. Nie, Current Opinion in Biotechnology 13, 40 (2002).
77. W. C. W. Chan, and S. Nie, Science 281, 2016 (1998).
78. D. Gerion, W. J. Parak, S. C. Williams, D. Zanchet, C. M. Micheel, and A. P. Alivisatos, J. Am. Chem. Soc. 124, 7070 (2002).
79. J. J. Storhoff, A. A. Lazarides, R. C. Mucic, C. A. Mirkin, R. L. Letsinger, and G. C. Schatz, J. Am. Chem. Soc. 122, 4640 (2000).

80. R. Jin, G. Wu, Z. Li, C. A. Mirkin, and G. C. Schatz, J. Am. Chem. Soc. 125, 1643 (2003).
81. C.-H. Kiang, Physica A 321, 164 (2003).
82. S. Link and M. A. El-Sayed, J. Phys. Chem. 103, 8410 (1999).
83. A. A. Lazarides and G. C. Schatz, J. Phys. Chem. 104, 460 (2000).
84. S. Y. Park and D. Stroud, Phys. Rev. B 67, 212202 (2003).
85. Y. Sun, N. C. Harris, and C.-H. Kiang, Physica A, to appear (2005).

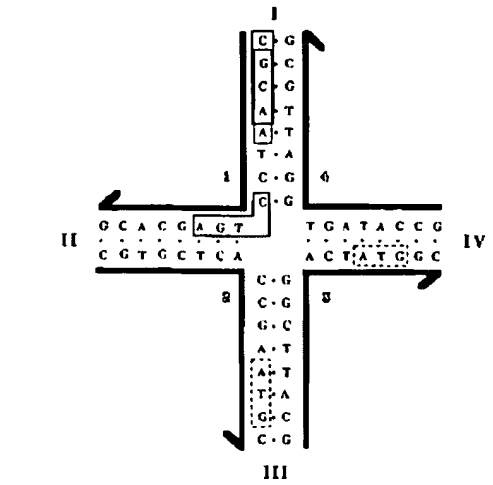

(a)

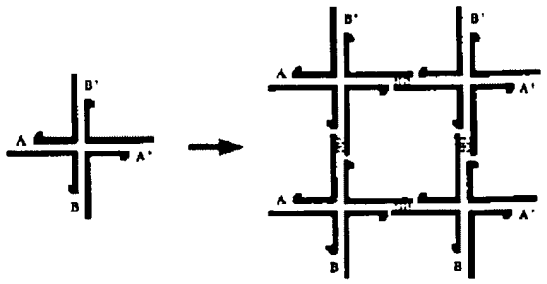

(b)

Fig. 1 (a) A four-armed stable branched DNA junction made by DNA molecules. (b) Use of the branched junctions to form periodic crystals. Reprinted from Ref. 12, N. C. Seeman, Nanotechnology 2, 149 (1991), with permission from Institute of Physics @ 1991 and Dr. Seeman.

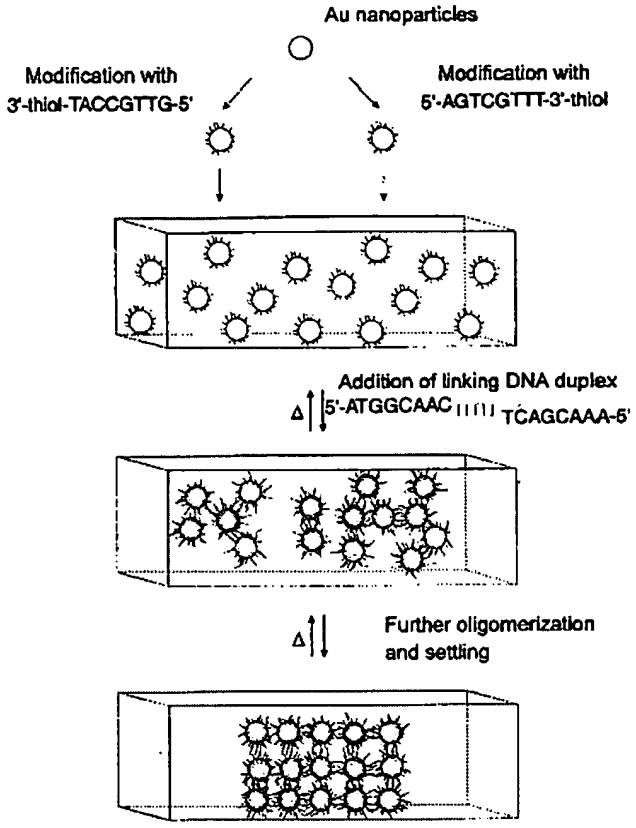

Fig. 2 Scheme showing the DNA-based gold nanoparticle assembly strategy. The scheme is not meant to imply the formation of a crystalline lattice but rather an aggregate structure that can be reversibly annealed. Reprinted from Ref. 16, C. A. Mirkin et al., Nature 382, 607 (1996), with permission from Nature Publishing Group @ 1996.

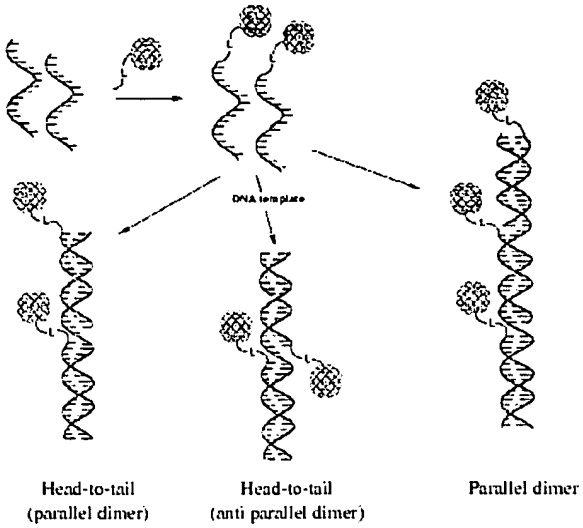

Fig. 3 Organize gold nanocrystals into spatially defined structures. Reprinted from Ref. 9, A. P. Alivisatos et al., Nature 382, 609 (1996), with permission from Nature Publishing Group @ 1996.

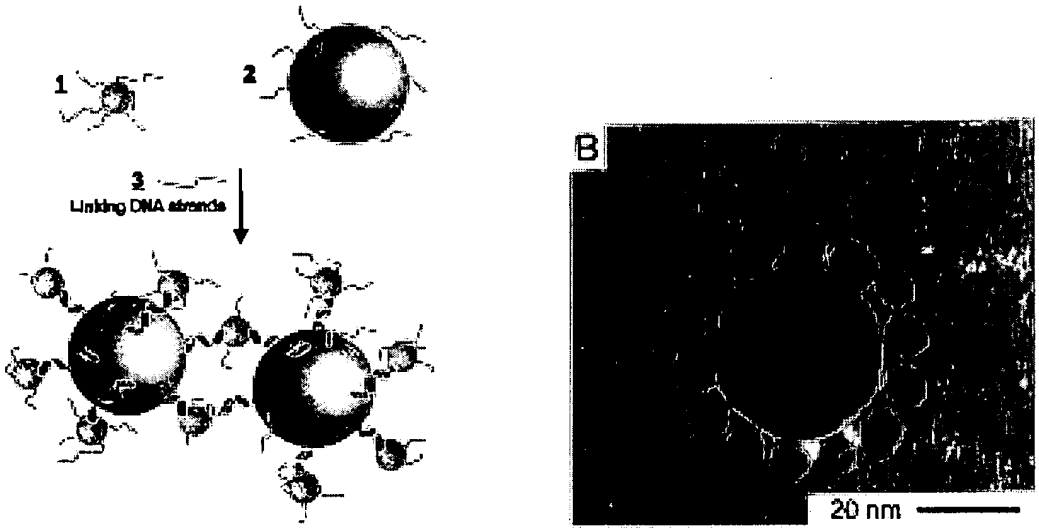

Fig. 4 DNA-directed synthesis of binary nanoparticle networks. The right panel shows a TEM image of a nanoparticle satellite structure. Reprinted from Ref. 18, R. C. Mucic et al., J. Am. Chem. Soc. 120, 12674 (1998), with permission from the American Chemical Society @ 1998.

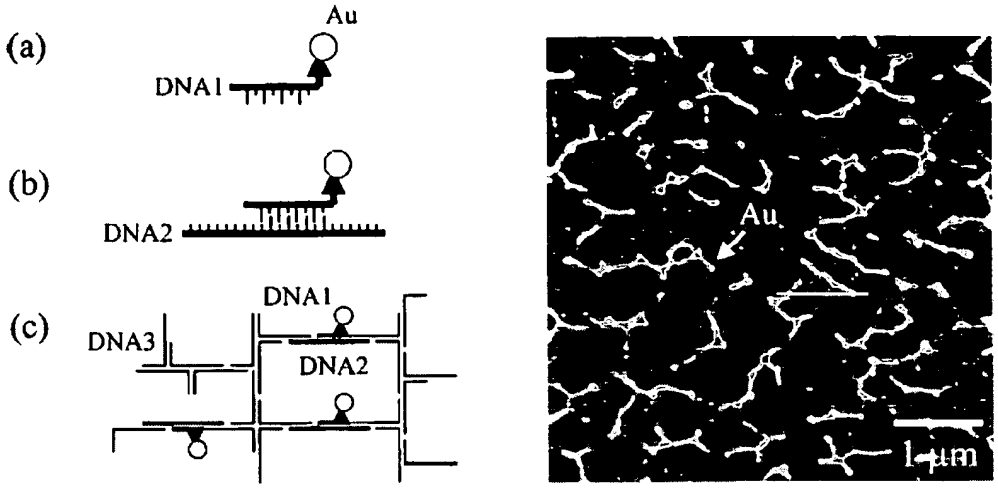

Fig. 5 (a) Approach for two-dimensional assembly of Au nanoparticles with a DNA network template. (b) AFM image of the Au-DNA network. Reprinted from Ref. 19, Y. Maeda et al., Appl. Phys. Lett. 79, 1181 (2001), with permission from American Institute of Physics @ 2001 and Dr. Kawai.

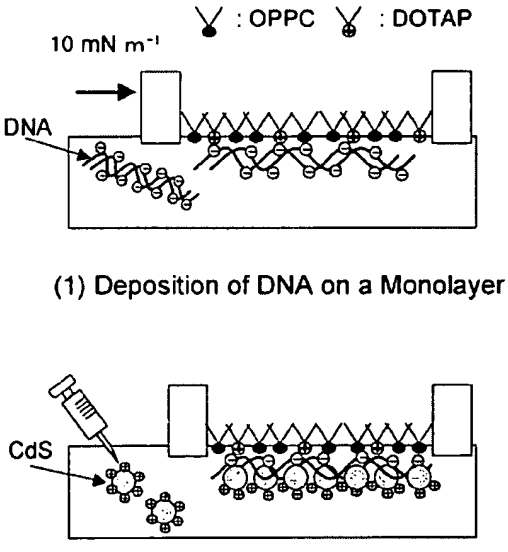

Fig. 6 Schematic illustration of the deposition of a CdS nanoparticle chain along a DNA molecule by using electrostatic interactions. Reprinted from Ref. 23, T. Torimoto et al., J. Phys. Chem. B, 103, 8799 (1999), with permission from the American Chemical Society @ 1999.

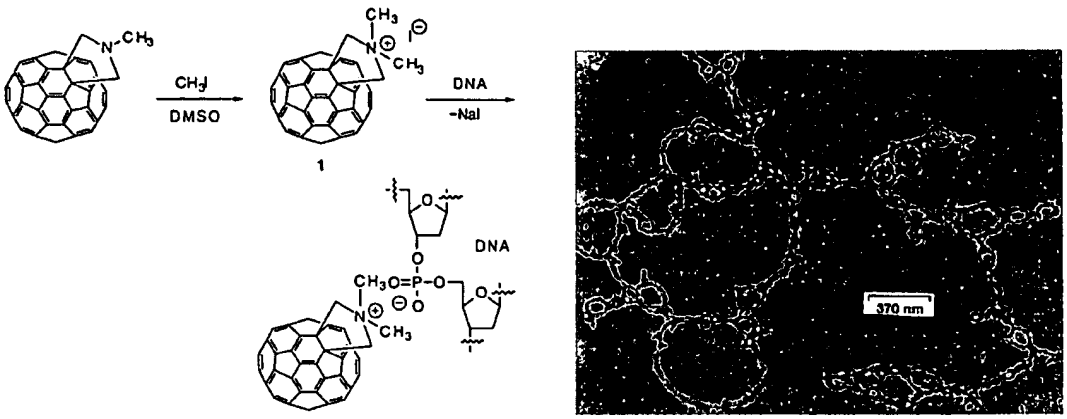

Fig. 7 Assembly of a DNA-fullerene hybrid. Reprinted from Ref. 26, A. M. Cassell et al., Angew. Chem., Int. Ed. 37, 1528 (1998), with permission from Wiley-VCH @ 1998 and Dr. Tour.

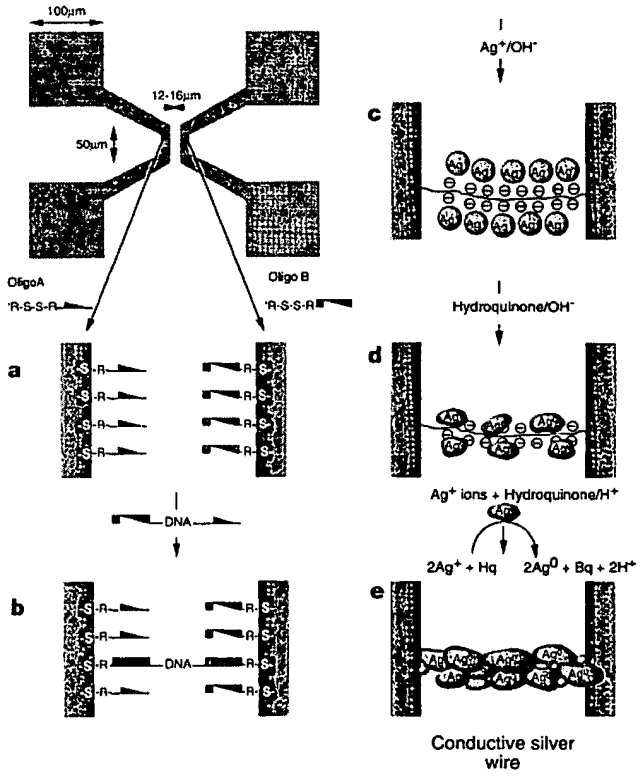

Fig. 8 DNA-templated assembly and electrode attachment of a conducting silver wire. Reprinted from Ref. 27, E. Braun et al., Nature 391, 775 (1998), with permission from Nature Publishing Group @ 1998.

Fig. 9 Fluorescence image of a DNA bridge connecting two gold electrodes. Reprinted from Ref. 27, E. Braun et al., Nature 391, 775 (1998), with permission from Nature Publishing Group @ 1998.

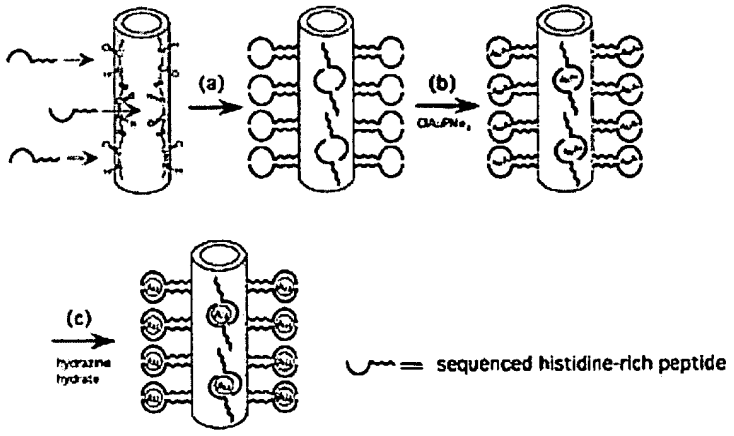

Fig. 10 Scheme for fabrication of Au nanowires using sequenced peptide nanotubes as templates. (a) Immobilization of the sequenced histidine-rich peptide at the amide binding sites of the template nanotubes. (b) Au ion immobilization on the sequenced histidine-rich peptide. (c) Au nanocrystal growth on the nanotubes nucleated at Au ion-binding sites after reducing Au ions with hydrazine hydrate. Reprinted from Ref. 31, R. Djalali, Y. Chen, and H. Matsui, J. Am. Chem. Soc. 125, 5873 (2003), with permission from the American Chemical Society @ 2003.

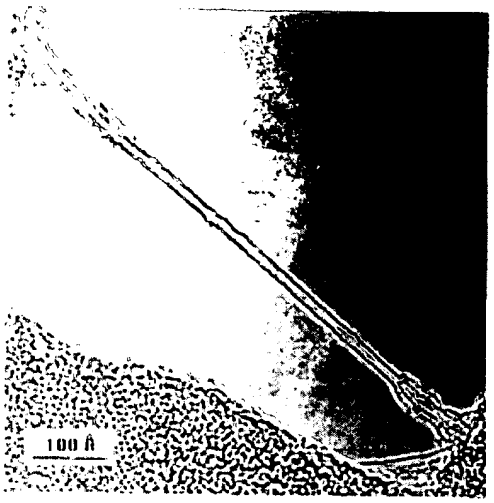

Fig. 11 TEM image of a single-walled carbon nanotube. Reprinted from Ref. 34, D. S. Bethune et al., Nature, (1993), with permission from Nature Publishing Group @ 1993.

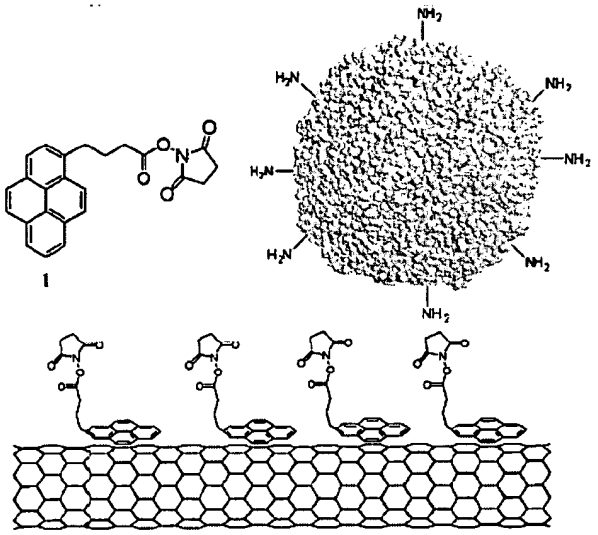

Fig. 12 Functionalization of SWNTs with succinimidyl ester groups. Reprinted from Ref. 46, R. J. Chen et al., J. Am. Chem. Soc. 123, 3838 (2001), with permission from the American Chemical Society @ 2001.

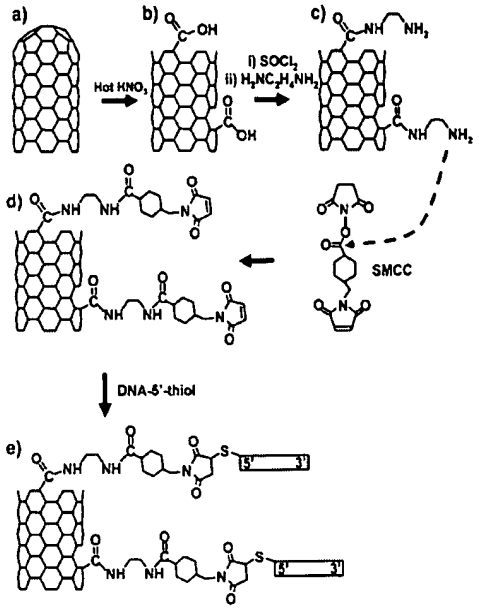

Fig. 13 An overview of the covalent attachment of DNA with SWNT. Reprinted from Ref. 48, S. E. Baker et al., Nano Lett. 2, 1413 (2002), with permission from the American Chemical Society @ 2002.

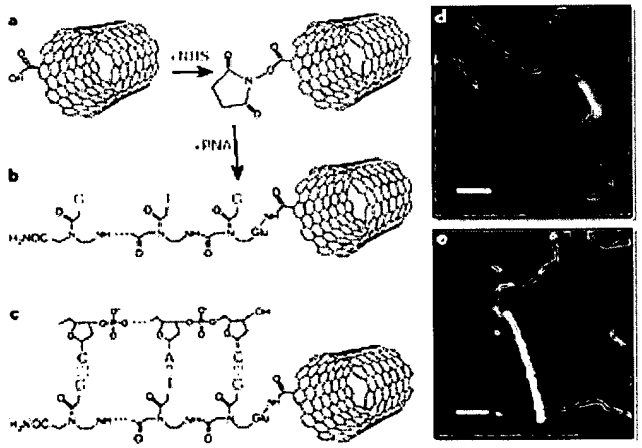

Fig. 14 Attachment of DNA to carbon nanotubes. **a, b,** N-hydroxysuccinimide (NHS) esters formed on carboxylated, SWNTs are displaced by peptide nucleic acid (PNA), forming an amide linkage. **c,** A DNA fragment with a single-stranded, 'sticky' end hybridizes by Watson–Crick base-pairing to the PNA–SWNT. **d, e,** Atomic-force microscope (TappingMode) images of PNA–SWNTs. Reprinted from Ref. 49, K. A. Williams et al., Nature 420, 761 (2002), with permission from Nature Publishing Group @ 2002.

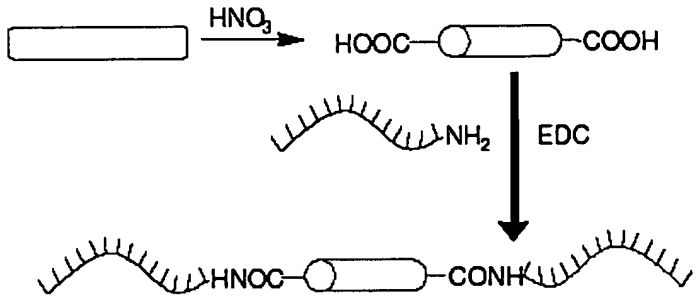

Fig. 15 The DNA/nanotube reaction scheme. Capped nanotubes are oxidatively opened and then reacted with amine-terminated single-stranded DNA. Reprinted from Ref. 51, C. Dwyer et al., Nanotechnology, 13, 601 (2002), with permission from Institute of Physics @ 2002 and Dr. Erie.

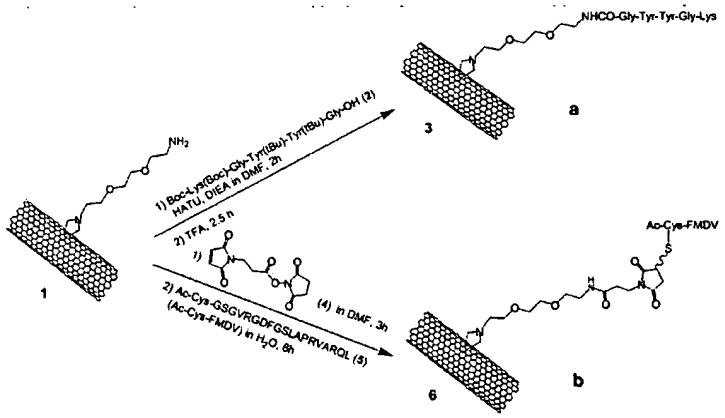

Fig. 16 Synthesis of the peptide-carbon nanotubes via (a) peptide fragment condensation and (b) chemoselective ligation. Reprinted from Ref. 53, D. Pantarotto et al., J. Am. Chem. Soc. 125, 6160 (2003), with permission from the American Chemical Society @ 2003.

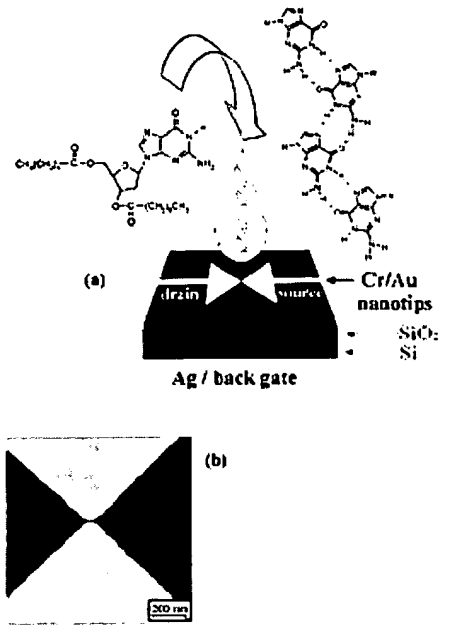

Fig. 17 A field effect transistor based on a modified DNA base. (a) Self-assembly and cast deposition of $dG(C_{10})_2$ on the three-terminal device, consisting of two arrowshaped Cr/Au (6 nm/35 nm thick) electrodes on a SiO_2 substrate and a third Ag back electrode (not to scale). (b) High magnification SEM image of two Cr/Au nanotips with separation of 20 nm. Reprinted from Ref. 54, G. Maruccio et al., Nano Lett. 3, 479 (2003), with permission from the American Chemical Society @ 2003.

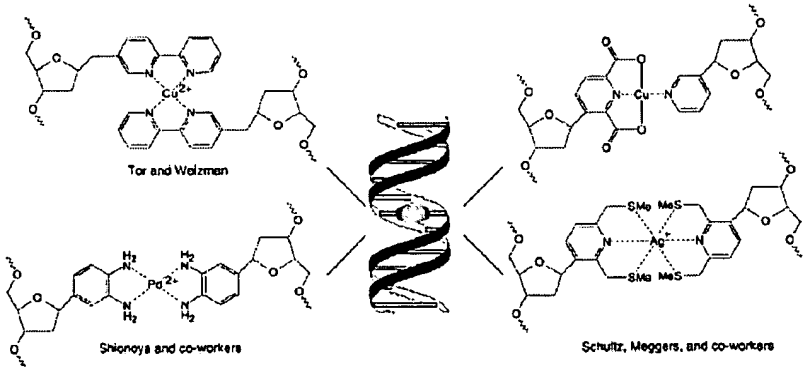

Fig. 18 Metal-ion-mediated base pairs replace natural base pairs in DNA duplexes. Reprinted from Ref. 58, H.-A. Wagenknecht, Angew. Chem. Int. Ed. 42, 3204 (2003), with permission from Wiley-VCH @ 2003.

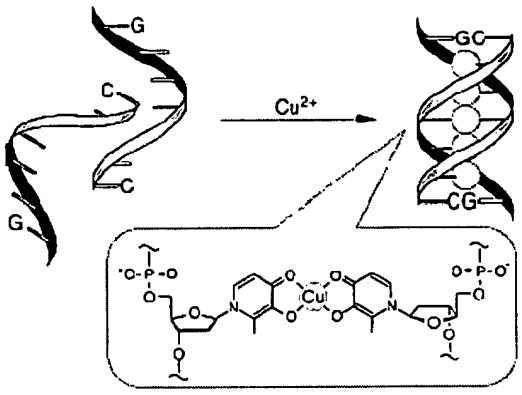

Fig. 19 Schematic representation of Cu-mediated duplex formation between two artificial DNA strands. Reprinted with permission from Ref. 65, K. Tanaka et al., Science 299, 1212 (2003). Copyright 2003 AAAS.

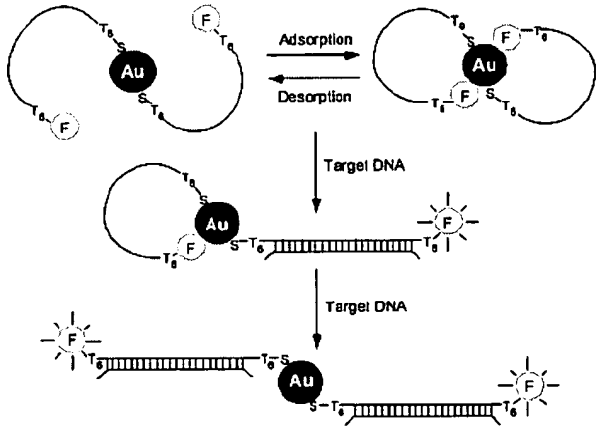

Fig. 20 Nanoparticle-based probes and their operating principles. Two oligonucleotide molecules are shown to self-assemble into a constrained conformation on each gold particle (2.5 nm diameter). A T6 spacer (six thymines) is inserted at both the 3′- and 5′-ends to reduce steric hindrance. Single-stranded DNA is represented by a single line and double-stranded DNA by a cross-linked double line. In the assembled (closed) state, the fluorophore is quenched by the nanoparticle. Upon target binding, the constrained conformation opens, the fluorophore leaves the surface because of the structural rigidity of the hybridized DNA (double-stranded), and fluorescence is restored. In the open state, the fluorophore is separated from the particle surface by about 10 nm. Au, gold particle; F, fluorophore; S, sulfur atom. Reprinted from Ref. 68, D. J. Maxwell et al., J. Am. Chem. Soc. 124, 9606 (2002), with permission from the American Chemical Society @ 2002.

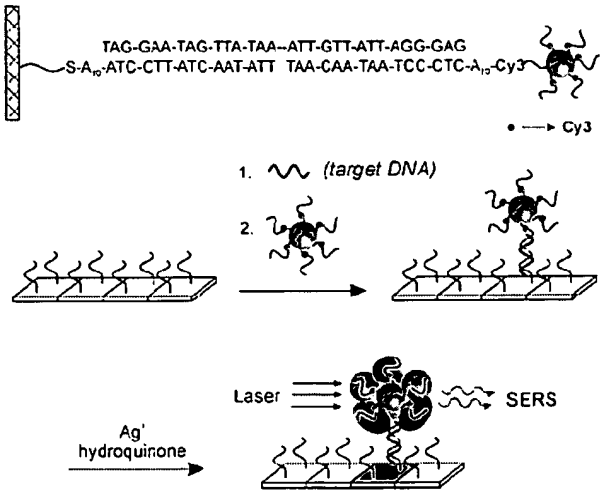

Fig. 21 Nanoparticles with Raman spectroscopic fingerprints for DNA and RNA detection. Reprinted with permission from Ref. 69, Y. Cao et al., Science 297, 1536 (2002). Copyright 2002 AAAS.

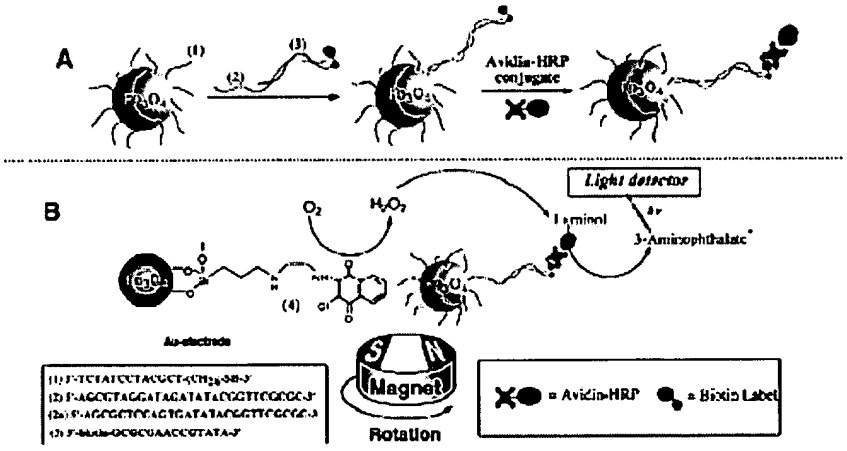

Fig. 22 (A) Preparation of DNA-functionalized magnetic particles labeled with the Avidin-HRP conjugate; (B) Amplified detection of DNA by the rotation of the labeled DNA-functionalized magnetic particles and quinone-modified magnetic particles by an external rotating magnet and the electrocatalyzed generation of chemiluminescence. Reprinted from Ref. 72, Weizmann et al., J. Am. Chem. Soc. 125, 3452 (2003), with permission from the American Chemical Society @ 2003.

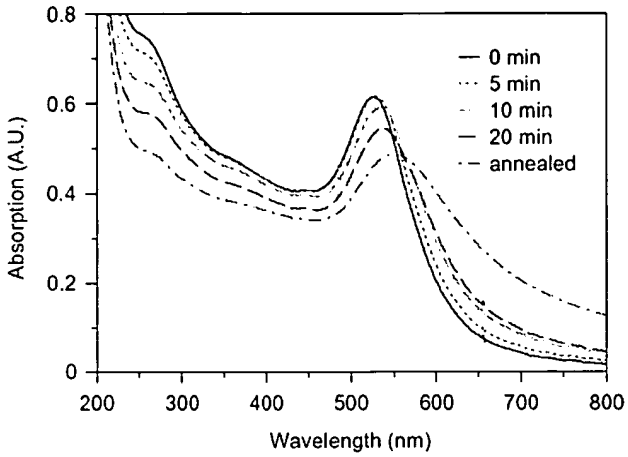

Fig. 23 Change of optical absorption spectra as a function of time of DNA-modified gold nanoparticles. Reprinted from Ref. 81, C.-H. Kiang, "Phase Transition of DNA-Linked Gold Nanoparticles," Physica A 321, 164, Copyright (2003), with permission from Elsevier.

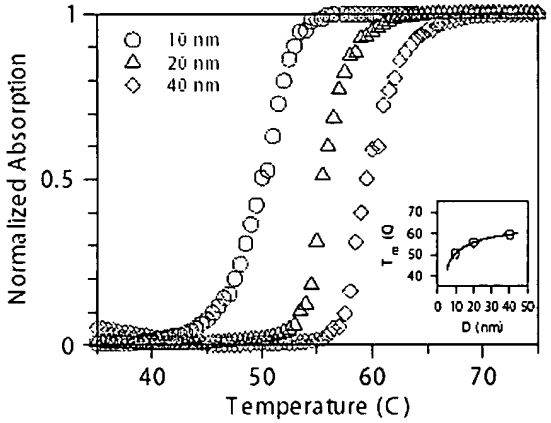

Fig. 24 Normalized melting curves of DNA-linked gold nanoparticle networks monitored at 260 nm. The inset shows the melting temperature as a function of particle diameter D. Reprinted from Ref. 81, C.-H. Kiang, "Phase Transition of DNA-Linked Gold Nanoparticles," Physica A 321, 164, Copyright (2003), with permission from Elsevier.